A numerical formulation and algorithm for limit and shakedown analysis of large-scale elastoplastic structures

Heng Peng[1], Yinghua Liu[1,*] and Haofeng Chen[2]

[1]Department of Engineering Mechanics, AML, Tsinghua University, Beijing 100084, People's Republic of China

[2]Department of Mechanical and Aerospace Engineering, University of Strathclyde, Glasgow G1 1XJ, UK

[*]Corresponding author: yhliu@mail.tsinghua.edu.cn

Abstract

In this paper, a novel direct method called the stress compensation method (SCM) is proposed for limit and shakedown analysis of large-scale elastoplastic structures. Without needing to solve the specific mathematical programming problem, the SCM is a two-level iterative procedure based on a sequence of linear elastic finite element solutions where the global stiffness matrix is decomposed only once. In the inner loop, the static admissible residual stress field for shakedown analysis is constructed. In the outer loop, a series of decreasing load multipliers are updated to approach to the shakedown limit multiplier by using an efficient and robust iteration control technique, where the static shakedown theorem is adopted. Three numerical examples up to about 140,000 finite element nodes confirm the applicability and efficiency of this method for two-dimensional and three-dimensional elastoplastic structures, with detailed discussions on the convergence and the accuracy of the proposed algorithm.

Keywords Direct method; Shakedown analysis; Stress compensation method; Large-scale; Elastoplastic structures

1 Introduction

In many fields of technology, such as petrochemical, civil, mechanical and space engineering, structures are usually subjected to variable repeated loading. The computation of the load-carrying capability of those structures beyond the elastic limit is an important but

difficult task in structural design and integrity assessment. The full step-by-step elastic-plastic analysis procedure may be used to estimate the long term behavior of a structure, such as shakedown, alternating plasticity, incremental plasticity or instantaneous collapse, by the acquired evolution of stresses and strains. Generally, the method is cumbersome and time-consuming, and needs the exact knowledge of the loading histories that often are uncertain in practical engineering situations. A better alternative is to perform the limit and shakedown analysis of structures using the direct methods [1,2], which just need to know the interval of these applied loads.

Most of the direct methods are based on the lower bound theorem by Melan [3] or the upper bound theorem by Koiter [4], both of which rest on the assumptions of perfectly plastic material, small displacements, negligible inertia and negligible creeping effects [5]. Since the two pioneering works, the subsequent researches have been along two different routes [6]. The first route of these researches is concerned with the extensions of shakedown theorem, where the material hardening [7-12], geometric nonlinearities [13,14], non-stationary loads [15,16], creeping effect [17,18] and frictional contact [19] are considered respectively. The second route of these researches is concerned with the development of efficient and robust numerical methods [20-30] towards the solution of the shakedown problem, which is also the major objective of this article.

Based on the lower or upper bound theorem, the limit and shakedown analysis of a structure is normally transformed into a mathematical programming problem that aims to minimize or maximize a goal function under excessive independent variables and constraint conditions. Different optimization approaches like the nonlinear Newton-type iteration algorithm [21,29,31], the second order cone programming (SQCP) [32,33] or the interior point method (IPM) [30,34-37] are widely used for solving the programming problem. Instead of using the standard finite element method, some researchers combine shakedown analysis with some other computational methods. The articles about the numerical shakedown analysis based on the boundary element method [38,39], the cell/edge/node-based smoothed element method (CS-FEM, ES-FEM or NS-FEM) [40-43], the element free method [44,45], the nodal natural element method [46,47] and the isogeometric analysis [48] are occasionally reported. However, when practical engineering problems are investigated, the finite element

discretization or the node arrangement will lead to a tremendous mathematical programming problem due to the significant number of variables and constraints, which may limit the application of these methods. In order to reduce the scale of the shakedown problem, some techniques such as the basis reduction technique [9,44,49] or subspace iteration are employed.

Noteworthy, although the numerical methods mentioned above are based on mathematical programming, there are some other approaches for limit and shakedown analysis in literatures. A group of elastic modulus adjustment methods [22-24,50-56], including the generalized local stress strain (GLOSS) r-node method [50], the m(alpha)-method [51], the elastic compensation method [22,23,52,53], and the linear matching method (LMM) [24,54-56], were systematically developed. Using more physical arguments, these methods match the linear behavior to the nonlinear plastic behavior by performing a sequence of linear solutions with spatially varying moduli. As the origin of these methods, the elastic compensation method (ECM) [52] was early put to use for calculating limit loads of pressure vessels. Then Ponter and Carter [22,23] demonstrated an initial implementation of this technique and also provided a rigorous theoretical proof for the existence of the monotonically reducing upper bounds. Finally, a more generalized and practical code called the LMM [24,55-58] was developed to be used for limit, shakedown and ratchet analyses of engineering structures by making full use of the commercial finite element software ABAQUS. Further, Garcea et al. [25,26] propsoed an incremental-iterative solution method which has analogies with the Riks path-following algorithm to plane frames and two-dimensional flat structures. Another direct method termed as the residual stress decomposition method for shakedown (RSDM-S) was presented [28]. Based on the cyclic nature of the residual stress in the steady cycle, the residual stress at every Gauss point is decomposed into Fourier series in time. This method was used for evaluating the shakedown loads of some simple two-dimensional structures.

As described above, both the traditional mathematical programming and iterative method with more physical agreements can be used for calculating the limit and shakedown loads. It is worth noting that many of the proposed methods appear to aim at academic purpose or to solve some specific simple problems but are not suitable for general engineering applications. Even through the shakedown analyses of some complex engineering structures using the IPM and the LMM were reported in recent years, the computing time of the IPM is still long when

solving large-scale shakedown problems and the finite element models reported in literatures have no more than 100,000 nodes. From the mathematical point of view, the elastic modulus adjustment method is not completely satisfactory, because it requires a complete elastic finite element analysis procedure that includes the assemblage of the stiffness matrix and its decomposition during every iteration [25].

In this work, a novel direct method named as the stress compensation method (SCM) for limit and shakedown analysis of large-scale engineering structures is proposed. The method adopts a two-level iterative strategy where a series of decreasing cyclic loading solutions based on linear elastic finite element analysis are generated. Over the numerical procedure, only one decomposition of the global stiffness matrix is required, and the residual stresses are directly calculated in a very small number of load vertices, which largely enhances the computational efficiency of the proposed algorithm. By using an efficient and robust iteration control technique, the convergence and the accuracy of the SCM are ensured. The layout of this paper is as follows: shakedown criterion and basic theorems for shakedown analysis are introduced in Sect. 2, followed by description of the formulation of the SCM in Sect. 3. Then the detailed numerical algorithm of the SCM for shakedown analysis is presented in Sect. 4. Three numerical examples including two-dimensional (2D) and three-dimensional (3D) large-scale engineering structures are considered to verify the availability of the proposed procedure, and the results are also compared to the reference solutions as well as calculations with the LMM and the step-by-step procedure to illustrate the accuracy and the efficiency of the SCM in Sect. 5. Finally, the discussion and conclusions are presented in Sect. 6.

2 Shakedown criterion and basic theorems

2.1 Static shakedown theorem by Melan

A lower bound evaluation of the load-carrying capability of an elastic-perfectly plastic structure under cyclic loading can be obtained by performing the shakedown analysis based on the static shakedown theorem. The classical conditions of shakedown theorem, such as small displacement gradient, time-independent material behavior without consideration of material damage and creeping effect, ignoring inertia effect are assumed here, although these

extensions are in reach. What's more, the convex yield surface and the normality rule are assumed so that the material is stable in Drucker's sense [30].

The statement of the static shakedown theorem is as follows [59]: a structure will shake down to the variable repeated loading, i.e. its behavior after a number of initial loading cycles will become purely elastic, if there exists a time-independent distribution of residual stress field $\boldsymbol{\rho}(\mathbf{x})$ such that its superposition with the fictitious elastic stress field $\boldsymbol{\sigma}^E(\mathbf{x},t)$, results in a safe stress state $\boldsymbol{\sigma}(\mathbf{x},t)$ at any point of the structure under any combination of loads inside the prescribed domain.

$$f\left(\boldsymbol{\sigma}(\mathbf{x},t)\right)=f\left(\boldsymbol{\sigma}^E(\mathbf{x},t)+\boldsymbol{\rho}(\mathbf{x})\right)\le 0 \qquad \forall \mathbf{x}\in\mathbf{V},\ \forall t \tag{1}$$

Here, $f(\cdot)$ is the yield function; $\boldsymbol{\sigma}(\mathbf{x},t)$ is the actual stress; $\boldsymbol{\sigma}^E(\mathbf{x},t)$ is the fictitious elastic stress that occurs if the structure responds to the prescribed loads in a purely elastic manner; $\boldsymbol{\rho}(\mathbf{x})$ represents a self-equilibrated residual stress field that should satisfy the equilibrium conditions within the body $\mathbf{V}$ and the boundary conditions on the part $\boldsymbol{\Gamma}_t$ of the surface, i.e.

$$\begin{aligned} \nabla\cdot\boldsymbol{\rho}&=\mathbf{0} \qquad \text{in } \mathbf{V}\\ \boldsymbol{\rho}\cdot\mathbf{n}&=\mathbf{0} \qquad \text{on } \boldsymbol{\Gamma}_t \end{aligned} \tag{2}$$

where $\nabla\cdot$ denotes the divergence operator; $\mathbf{n}$ is the unit outward normal to the boundary $\boldsymbol{\Gamma}_t$.

2.2 Load domain and specified loading path

Structures are often subjected to many types of loads at the same time, and generally, the loads vary randomly. If a finite number of the external loads obeying their own rules vary in a domain, the loading history $\mathbf{P}(\mathbf{x},t)$ can be described as the superposition of these external loads with different loading sets $\mathbf{P}_i(\mathbf{x},t),\ (i=1,\cdots,N)$. The each loading set $\mathbf{P}_i(\mathbf{x},t)$ can be decided by time-dependent multiplier $\mu_i(t)$ and the normalized basis load $\mathbf{P}_i^0(\mathbf{x})$.

$$\mathbf{P}(\mathbf{x},t)=\sum_{i=1}^{N}\mathbf{P}_i(\mathbf{x},t)=\sum_{i=1}^{N}\mu_i(t)\mathbf{P}_i^0(\mathbf{x}) \tag{3}$$

Considering the bound values of each multiplier are given as follows:

$$\mu_i^- \le \mu_i(t) \le \mu_i^+ \tag{4}$$

Eq. (3) describes a domain $\mathbf{\Omega}$ of these loads. The load domain $\mathbf{\Omega}$ is a polyhedron defined by *m* vertices $B^1, B^2, \cdots, B^m$ in the space of load parameters. It is worth noting that the load domain $\mathbf{\Omega}$ may not be convex and the detailed descriptions of load domain for complex load conditions can be seen in Ref. [60]. As shown in Fig. 1(a), a load domain with five load vertices is taken as an example.

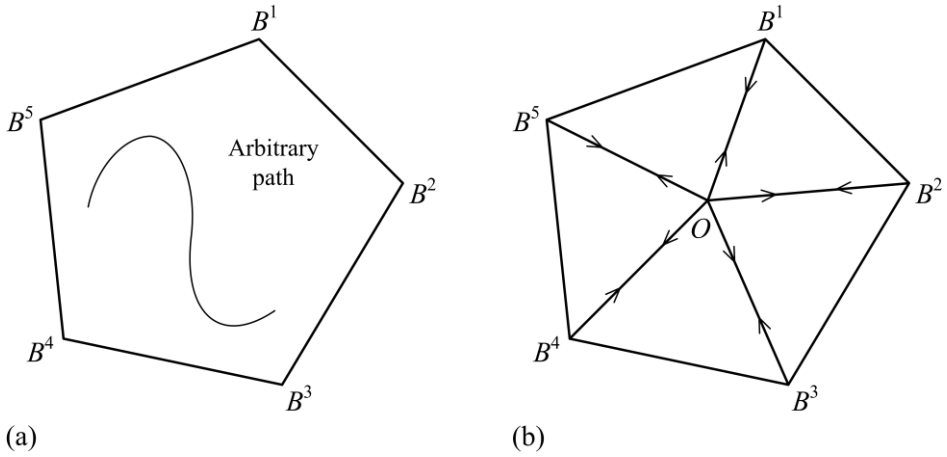

Fig. 1 Load domain and loading path: (a) arbitrary loading path; (b) specified loading path

Although the exact loading history is unknown and the loads may vary in an arbitrary manner within a domain $\mathbf{\Omega}$, the domain $\mathbf{\Omega}$ is usually known in practical engineering problems. In order to determine the shakedown behavior of the structure under the load domain $\mathbf{\Omega}$, König [5] proposed a relevant theorem which is stated as follows:

If a given structure shakes down over a certain cyclic loading path which contains all the *m* vertices $B^1, B^2, \cdots, B^m$ of the hyper-polyhedral load domain $\mathbf{\Omega}$, the structure shakes down in an arbitrary loading history defined by Eq. (3).

On the other hand, if the structure does not shake down in a certain cyclic loading path containing some of the vertices, the direct evidence can be obtained so that the domain $\mathbf{\Omega}$ is not a shakedown domain of the structure.

The above statement provides a good strategy to estimate whether or not a given structure will shake down over any loading path within the domain $\mathbf{\Omega}$. We define a specified loading path $\bar{\mathbf{P}}(t)$ which contains all the vertices of the hyper-polyhedral load domain $\mathbf{\Omega}$, as

illustrated in Fig. 1(b). If the structure shakes down under this loading path, then it must shake down within the load domain defined by all these vertices.

It should be pointed out here that the shakedown analysis will degenerate to the limit analysis and the plastic limit load can be calculated when the number of the vertices of the load domain equals to one.

2.3 Steady cyclic stress state

We assume that a body of volume V is subjected to cyclic mechanical loads on a part of the surface S. The expression of the mechanical loads is as follows:

$$\mathbf{P}(\mathbf{x},t)=\mathbf{P}(\mathbf{x},t+nT) \tag{5}$$

where $\mathbf{P}(\mathbf{x},t)$ has the same definition as that in Eq. (3); t is the current time point measured from the beginning of the cycle; T is the period of the cycle; $n=1, 2, \cdots$ denotes the number of full cycles; $\mathbf{x}$ denotes the coordinates of a material point in the body.

We suppose that the material of a structure is elastic-perfectly plastic and obeys the Drucker's postulate. The actual stress $\boldsymbol{\sigma}(\mathbf{x},t)$ in the structure is decomposed into two parts: the fictitious elastic stress part $\lambda^{(k)}\boldsymbol{\sigma}^E(\mathbf{x},t)$ and the residual stress part $\boldsymbol{\rho}(\mathbf{x},t)$, i.e.

$$\boldsymbol{\sigma}(\mathbf{x},t)=\lambda^{(k)}\boldsymbol{\sigma}^E(\mathbf{x},t)+\boldsymbol{\rho}(\mathbf{x},t) \tag{6}$$

where $\lambda^{(k)}$ is a load multiplier.

The corresponding strain rate can also be decomposed into two parts:

$$\dot{\boldsymbol{\varepsilon}}(\mathbf{x},t)=\lambda^{(k)}\dot{\boldsymbol{\varepsilon}}^E(\mathbf{x},t)+\dot{\boldsymbol{\varepsilon}}_r(\mathbf{x},t) \tag{7}$$

where the first term $\dot{\boldsymbol{\varepsilon}}^E(\mathbf{x},t)$ on the right of the equation is the elastic strain rate corresponding to the fictitious elastic stress rate $\dot{\boldsymbol{\sigma}}^E(\mathbf{x},t)$ and the second term $\dot{\boldsymbol{\varepsilon}}_r(\mathbf{x},t)$ on the right of the equation is the residual strain rate. It should be noted that the residual strain rate $\dot{\boldsymbol{\varepsilon}}_r(\mathbf{x},t)$ consists of the plastic part $\dot{\boldsymbol{\varepsilon}}^p(\mathbf{x},t)$ and the elastic part $\dot{\boldsymbol{\varepsilon}}_r^e(\mathbf{x},t)$, and $\dot{\boldsymbol{\varepsilon}}_r^e(\mathbf{x},t)$ is required so that the total strain rate $\dot{\boldsymbol{\varepsilon}}(\mathbf{x},t)$ satisfies the deformation compatibility over the whole body. Then, Eq. (7) can be written as

$$\dot{\boldsymbol{\varepsilon}}(\mathbf{x},t)=\lambda^{(k)}\dot{\boldsymbol{\varepsilon}}^E(\mathbf{x},t)+\dot{\boldsymbol{\varepsilon}}^p(\mathbf{x},t)+\dot{\boldsymbol{\varepsilon}}_r^e(\mathbf{x},t) \tag{8}$$

According to the constitutive law of the elastic-perfectly plastic material with an associated flow rule, the following equations are obeyed:

$$\dot{\boldsymbol{\sigma}}^{E}\left(\mathbf{x},t\right)=\mathbf{D}\cdot\dot{\boldsymbol{\varepsilon}}^{E}\left(\mathbf{x},t\right) \tag{9}$$

$$\dot{\boldsymbol{\rho}}\left(\mathbf{x},t\right)=\mathbf{D}\cdot\dot{\boldsymbol{\varepsilon}}_{r}^{e}\left(\mathbf{x},t\right) \tag{10}$$

$$\dot{\boldsymbol{\varepsilon}}^{p}\left(\mathbf{x},t\right)=\alpha\frac{\partial f}{\partial\boldsymbol{\sigma}\left(\mathbf{x},t\right)} \tag{11}$$

where **D** is the elastic stiffness matrix; *f* is the yield function; $\dot{\boldsymbol{\varepsilon}}^{p}\left(\mathbf{x},t\right)$ is the plastic strain rate whose direction is along the outer normal of the yield surface; and α is the plastic multiplier. Because of the convexity of the yield surface, the following inequality holds referring to the Drucker's postulate:

$$\left(\boldsymbol{\sigma}-\boldsymbol{\sigma}^{a}\right)\cdot\dot{\boldsymbol{\varepsilon}}^{p}\geq 0 \tag{12}$$

where $\boldsymbol{\sigma}$ is the stress at yield surface associated with the plastic strain rate $\dot{\boldsymbol{\varepsilon}}^{p}$ and $\boldsymbol{\sigma}^{a}$ is an admissible stress.

It has been elucidated [59,61,62] that a cyclically loaded elastoplastic structure made up of material obeying Drucker's postulate will reach a steady cyclic state, that is, the stresses and the strain rates will gradually stabilize from cycle to cycle. The stress distribution in the steady cycle does not depend upon the initial stress state and is unique in those regions where the plastic strain rates are non-vanishing [59]. However, it should be noted that the time-independent residual stress field within the elastic regions in the steady cyclic state is not unique [62].

3 Description of the SCM

To provide simply and rapidly the steady cyclic stress state for an elastic-perfectly plastic structure with von Mises yield model, the stress compensation method abbreviated with the SCM is presented here.

We suppose that a structure is discretized into finite element meshes. All the strains and the stresses are calculated at the Gauss points of the element. The strain rate $\dot{\boldsymbol{\varepsilon}}\left(\mathbf{x},t\right)$ at the Gauss point is related to the nodal displacement rate $\dot{\mathbf{u}}\left(t\right)$ of the element:

$$\dot{\boldsymbol{\varepsilon}}(\mathbf{x},t)=\mathbf{B}(\mathbf{x})\cdot\dot{\mathbf{u}}(t) \tag{13}$$

where $\mathbf{B}(\mathbf{x})$ is the strain-displacement matrix.

Substituting Eq. (8) into (10), the residual stress rate $\dot{\boldsymbol{\rho}}(\mathbf{x},t)$ at the Gauss point is written as

$$\dot{\boldsymbol{\rho}}(\mathbf{x},t)=\mathbf{D}\cdot\left(\dot{\boldsymbol{\varepsilon}}(\mathbf{x},t)-\lambda^{(k)}\dot{\boldsymbol{\varepsilon}}^{E}(\mathbf{x},t)-\dot{\boldsymbol{\varepsilon}}^{p}(\mathbf{x},t)\right) \tag{14}$$

Since the residual stress rate field $\dot{\boldsymbol{\rho}}(\mathbf{x},t)$ is self-equilibrated and the strain rate $\dot{\boldsymbol{\varepsilon}}(\mathbf{x},t)$ is kinematically admissible, the principle of virtual work can be adopted as follows:

$$\int_V \delta\dot{\boldsymbol{\varepsilon}}^{\mathrm{T}}(\mathbf{x},t)\cdot\dot{\boldsymbol{\rho}}(\mathbf{x},t)dV=0 \tag{15}$$

where the superscript T denotes the symbol of transpose and $\delta\dot{\boldsymbol{\varepsilon}}(\mathbf{x},t)$ is the virtual strain rate.

Substituting Eqs. (13) and (14) into Eq. (15), we get

$$\delta\dot{\mathbf{u}}^{\mathrm{T}}(t)\cdot\left(\int_V \mathbf{B}^{\mathrm{T}}\cdot\mathbf{D}\cdot\left(\mathbf{B}\cdot\dot{\mathbf{u}}(t)-\lambda^{(k)}\dot{\boldsymbol{\varepsilon}}^{E}(\mathbf{x},t)-\dot{\boldsymbol{\varepsilon}}^{p}(\mathbf{x},t)\right)dV\right)=0 \tag{16}$$

Since Eq. (16) holds for any virtual displacement rate $\delta\dot{\mathbf{u}}(t)$, the integral formula consisting in this equation must vanish, that is

$$\left(\int_V \mathbf{B}^{T}\cdot\mathbf{D}\cdot\mathbf{B}dV\right)\cdot\dot{\mathbf{u}}(t)=\lambda^{(k)}\int_V \mathbf{B}^{T}\cdot\mathbf{D}\cdot\dot{\boldsymbol{\varepsilon}}^{E}(\mathbf{x},t)dV+\int_V \mathbf{B}^{T}\cdot\mathbf{D}\cdot\dot{\boldsymbol{\varepsilon}}^{p}(\mathbf{x},t)dV \tag{17}$$

For an elastoplastic structure, the exact solution of the plastic strain rate $\dot{\boldsymbol{\varepsilon}}^{p}(\mathbf{x},t)$ may be obtained by the elastic-plastic analysis using the traditional incremental method. Instead, we adopt another approach [28] to deal with it here. We replace the term $\mathbf{D}\cdot\dot{\boldsymbol{\varepsilon}}^{p}(\mathbf{x},t)$ with $\boldsymbol{\sigma}^{C}(\mathbf{x},t)$ which is named as the compensation stress in this article, and substitute Eqs. (9) and (13) into (17) and (14). Then Eqs. (17) and (14) give, respectively

$$\mathbf{K}\cdot\dot{\mathbf{u}}(t)=\lambda^{(k)}\int_V \mathbf{B}^{T}\cdot\dot{\boldsymbol{\sigma}}^{E}(\mathbf{x},t)dV+\int_V \mathbf{B}^{T}\cdot\boldsymbol{\sigma}^{C}(\mathbf{x},t)dV \tag{18}$$

$$\dot{\boldsymbol{\rho}}(\mathbf{x},t)=\mathbf{D}\cdot\mathbf{B}\cdot\dot{\mathbf{u}}(t)-\lambda^{(k)}\dot{\boldsymbol{\sigma}}^{E}(\mathbf{x},t)-\boldsymbol{\sigma}^{C}(\mathbf{x},t) \tag{19}$$

where $\mathbf{K}=\int_V \mathbf{B}^{T}\cdot\mathbf{D}\cdot\mathbf{B}dV$ is the global stiffness matrix of the structure. The value of $\boldsymbol{\sigma}^{C}(\mathbf{x},t)$ may be obtained by performing the iterative procedure as follows.

For the iteration *n*:

1) The total stresses at all the Gauss points in a body are calculated for a given load vertex of the specified loading path.

$$\boldsymbol{\sigma}^{(n)}(\mathbf{x},t)=\lambda^{(k)}\boldsymbol{\sigma}^{E}(\mathbf{x},t)+\boldsymbol{\rho}^{(n)}(\mathbf{x},t) \tag{20}$$

2) We check whether the total stress $\boldsymbol{\sigma}^{(n)}(\mathbf{x},t)$ exceeds the von Mises yield surface at every Gauss point in the body. As illustrated in Fig. 2, the sum of the residual stress vector $\overrightarrow{OD}$ ($\boldsymbol{\rho}(\mathbf{x},t)$) and the fictitious elastic stress vector $\overrightarrow{DC}$ ($\lambda^{(k)}\boldsymbol{\sigma}^{E}(\mathbf{x},t)$) is the total stress vector $\overrightarrow{OC}$ ($\boldsymbol{\sigma}^{(n)}(\mathbf{x},t)$). The part in excess of the von Mises yield surface is the compensation stress vector $\overrightarrow{AC}$ ($\boldsymbol{\sigma}^{C(n)}(\mathbf{x},t)$) which is calculated by the following formulae:

$$\begin{aligned}&\boldsymbol{\sigma}^{C(n)}(\mathbf{x},t)=\xi^{(n)}(\mathbf{x},t)\cdot\boldsymbol{\sigma}^{(n)}(\mathbf{x},t),\\&\xi^{(n)}(\mathbf{x},t)=\begin{cases}\dfrac{\bar{\sigma}^{(n)}(\mathbf{x},t)-\sigma_y}{\bar{\sigma}^{(n)}(\mathbf{x},t)} & \left(\bar{\sigma}^{(n)}(\mathbf{x},t)>\sigma_y\right)\\ 0 & \left(\bar{\sigma}^{(n)}(\mathbf{x},t)\le\sigma_y\right)\end{cases}\end{aligned} \tag{21}$$

3) Substituting Eq. (21) into (18), the nodal displacement rate $\dot{\mathbf{u}}^{(n)}(t)$ is obtained by solving the equilibrium equations in Eq. (22). The residual stress rate can be calculated by Eq. (23). Then the residual stress $\boldsymbol{\rho}^{(n)}(\mathbf{x},t)$ for the next load vertex can be updated by Eq. (24).

$$\mathbf{K}\cdot\dot{\mathbf{u}}^{(n)}(t)=\lambda^{(k)}\int_V\mathbf{B}^T\cdot\dot{\boldsymbol{\sigma}}^{E}(\mathbf{x},t)dV+\int_V\mathbf{B}^T\cdot\boldsymbol{\sigma}^{C(n)}(\mathbf{x},t)dV \tag{22}$$

$$\dot{\boldsymbol{\rho}}^{(n)}(\mathbf{x},t)=\mathbf{D}\cdot\mathbf{B}\cdot\dot{\mathbf{u}}^{(n)}(t)-\lambda^{(k)}\dot{\boldsymbol{\sigma}}^{E}(\mathbf{x},t)-\boldsymbol{\sigma}^{C(n)}(\mathbf{x},t) \tag{23}$$

$$\boldsymbol{\rho}^{(n)}(\mathbf{x},t+\Delta t)=\boldsymbol{\rho}^{(n)}(\mathbf{x},t)+\int_t^{t+\Delta t}\dot{\boldsymbol{\rho}}^{(n)}(\mathbf{x},t)dt \tag{24}$$

4) Repeat steps 1-3 for every load vertex.

5) Check the convergence of the value of compensation stress, and repeat the steps 1-4 till the convergence of iteration is achieved.

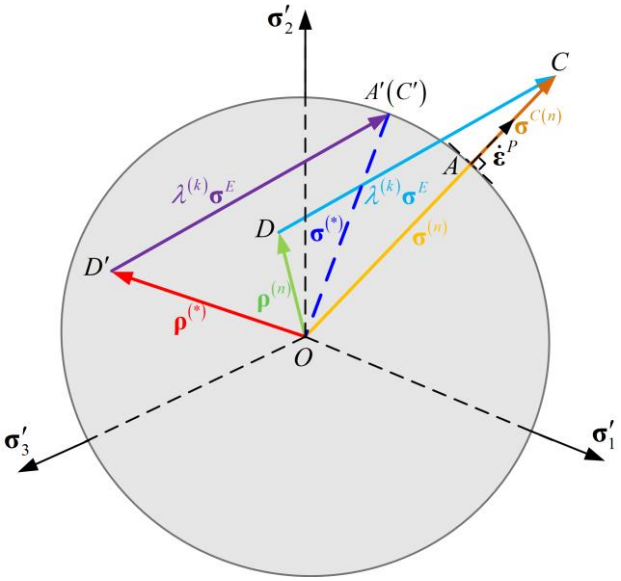

Fig. 2 von Mises yield surface and stress superposition schematic in the deviatoric plane

According to the theorem on existence and uniqueness of a steady stress cycle by Gokhfeld and Cherniavsky [59], the above procedure will evaluate a steady cyclic stress state of the structure, and the evolution of compensation stress $\boldsymbol{\sigma}^C(\mathbf{x},t)$ is also obtained. It should be noted that although the value of $\boldsymbol{\sigma}^C(\mathbf{x},t)$ may be different from that of $\mathbf{D}\cdot\dot{\boldsymbol{\varepsilon}}^p(\mathbf{x},t)$, they are going to vanish at the same time if it happens. Thus, the compensation stress can be considered as a symbol for estimating whether the structure shakes down, i.e., whether the structure responds to the subsequent cyclic loads in a purely elastic manner.

4 Numerical algorithm of the SCM for shakedown analysis

As discussed in Sect. 2, the shakedown behavior of a structure subjected to repeated loads varying arbitrarily in a load domain can be determined by estimating the behavior of the structure under a specified loading path which includes all the load vertices, and the existence of the steady cyclic stress state of a structure with the elastic-perfectly plastic material obeying the Drucker's postulate is demonstrated. Instead of using a standard elastic-plastic finite element analysis, an approximated steady cyclic stress state is assessed by using the SCM, as elaborated in Sect. 3.

In this section, a numerical procedure well suitable for shakedown analysis is proposed by performing a sequence of linear elastic finite element analyses over some cyclic loading

process, and the flowchart of the procedure is illustrated in Fig. 3.

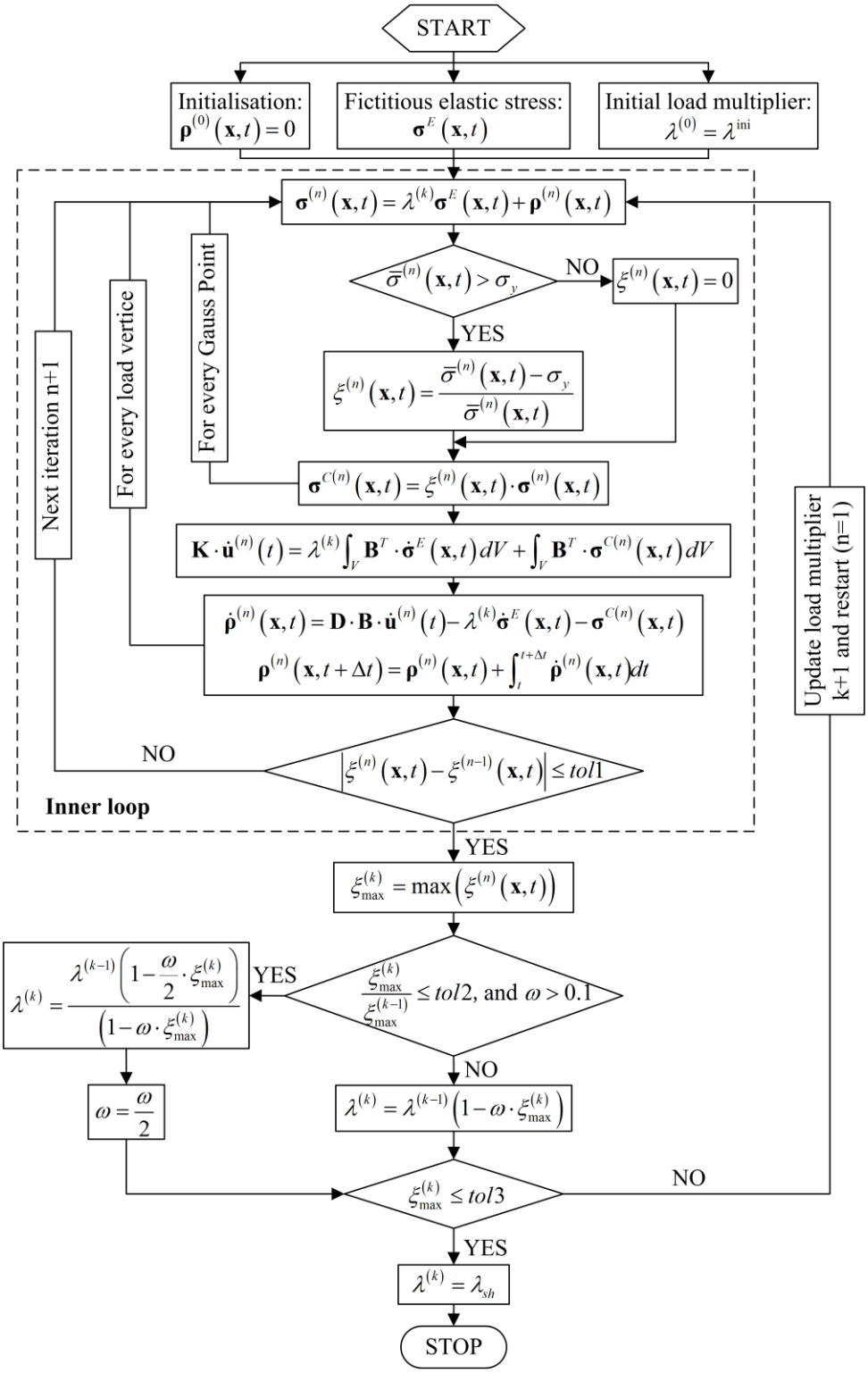

Fig. 3 Flowchart of the proposed SCM procedure for shakedown analysis

4.1 Evaluation of an initial load multiplier

The numerical procedure commences by calculating the fictitious elastic stress field $\boldsymbol{\sigma}^E(\mathbf{x},t)$ at each extreme point in the specified loading path and by constructing an initial load multiplier λ^{ini}. The fictitious elastic stress field can be easily obtained via the elastic finite element analysis. However, the initial load multiplier must be chosen as a value above the shakedown limit, from which the decreasing load multiplier may be generated after each outer iteration. According to the description in Ref. [24], the upper bound load multiplier

$$\lambda^{\text{ini}} = \frac{\int_V \left(\sigma_y \sum_{i=1}^{m} \bar{\varepsilon}_i(\mathbf{x}) \right) dV}{\int_V \left(\sum_{i=1}^{m} \boldsymbol{\sigma}^E(\mathbf{x},t_i) \cdot \boldsymbol{\varepsilon}^E(\mathbf{x},t_i) \right) dV} \tag{25}$$

must be an appropriate initial load multiplier. Here, $\boldsymbol{\varepsilon}^E(\mathbf{x},t_i)$ is the elastic strain corresponding to the fictitious elastic stress $\boldsymbol{\sigma}^E(\mathbf{x},t_i)$ at load vertex t_i, m is the number of the load vertices, and $\bar{\varepsilon}_i(\mathbf{x})$ is the effective strain of $\boldsymbol{\varepsilon}^E(\mathbf{x},t_i)$.

4.2 The proposed numerical procedure for shakedown analysis

As illustrated in Fig. 3, the procedure consists of two iteration loops. The inner one controlled by iteration *n* is used to obtain the approximately steady cyclic stress, and the outer one controlled by iteration *k* is used to calculate the shakedown load multiplier.

For the inner loop, the value of $\xi^{(n)}(\mathbf{x},t)$ (Eq. (21)) is examined:

$$\left| \xi^{(n)}(\mathbf{x},t) - \xi^{(n-1)}(\mathbf{x},t) \right| \le tol1 \tag{26}$$

where *tol*1 is a tolerance parameter which dynamically reduces from 10^{-3} to 10^{-4} according to the value of $\xi^{(n)}(\mathbf{x},t)$. The maximum value of $\xi^{(n)}(\mathbf{x},t)$ at all the Gauss points for all load vertices is updated at the end of each loading cycle, that is

$$\xi_{\max}^{(k)} = \max\left(\xi^{(n)}(\mathbf{x},t) \right) \tag{27}$$

where $\xi_{\max}^{(k)}$ is the maximum value during the outer iteration *k*.

Before calculating the load multiplier by the following expression:

$$\lambda^{(k)} = \lambda^{(k-1)}\left(1-\omega\cdot\xi_{\max}^{(k)}\right) \tag{28}$$

where ω is a convergence parameter with an initial value 0.1~0.5, $\lambda^{(k-1)}$ is the previous load multiplier and $\lambda^{(k)}$ is the updated load multiplier, a probable overshooting below shakedown limit will be examined by the following judgment:

$$\frac{\xi_{\max}^{(k)}}{\xi_{\max}^{(k-1)}} \le tol2, \text{ and } \omega > 0.1 \tag{29}$$

where *tol*2 usually takes 0.1~0.2; the initial value of $\xi_{\max}^{(0)}$ is 1.0. If Condition (29) is satisfied, the previous load multiplier must be modified by

$$\lambda^{(k)} = \frac{\lambda^{(k-1)}\left(1-\frac{\omega}{2}\cdot\xi_{\max}^{(k)}\right)}{\left(1-\omega\cdot\xi_{\max}^{(k)}\right)} \tag{30}$$

and then the convergence parameter ω is halved:

$$\omega = \frac{\omega}{2} \tag{31}$$

In final, a desired tolerance *tol*3 (e.g. 10^{-4}~10^{-3}) is given to estimate whether $\xi_{\max}^{(k)}$ approaches to zero or not

$$\xi_{\max}^{(k)} \le tol3 \tag{32}$$

If Condition (32) is satisfied, it means that the calculated load multiplier becomes the shakedown limit multiplier λ_{sh}, i.e.

$$\lambda^{(k)} = \lambda_{sh} \tag{33}$$

otherwise, a new outer iteration starts and the inner iteration number resets to 1. In fact, the criterion shown in Condition (32) is equivalent to the following form:

$$\left|\frac{\lambda^{(k)}-\lambda^{(k-1)}}{\lambda^{(k-1)}}\right| \le \omega\cdot\xi_{\max}^{(k)} \tag{34}$$

where the value of ω is not more than 0.5. Thus, the relative error of the calculated shakedown limit multiplier is not more than 0.1%.

4.3 Convergence and accuracy considerations

An iterative strategy shown in Eq. (28) will allow the proposed procedure to produce a sequence of decreasing cyclic loading solutions and to end up with the limiting value of loading parameters at which shakedown takes place. The relevant mathematical proof on the uniqueness of stress state at the limiting cycle has been presented by Gokhfeld and Cherniavsky [59]. Thus, if the iterative control technique and some tolerance parameters are adopted appropriately in the SCM procedure, a series of decreasing load multipliers will approach smoothly to the shakedown limit multiplier.

The value of *tol*1 used to control and stop the inner loop is a key factor that influences the accuracy and efficiency of the algorithm. Considering that the accuracy of the calculated shakedown limit multiplier is mainly determined by the finally convergent solution and has little relation to the solution in the intermediate process, a dynamically varying value of *tol*1 is used to balance the accuracy and the efficiency. A final value of $tol1 = 10^{-4}$ proves enough for a good calculation accuracy of the steady stress cycle.

The iteration strategy shown in Eq. (28) with $\omega = 0.5$ might not strictly prohibit the load multiplier from overshooting below the target solution at shakedown. To deal with this problem, the numerical scheme shown through Eqs. (29)-(31) is followed, and then even though the overshooting might still occur, its value must be small enough to be ignored. Once Condition (29) is satisfied, the calculated load multiplier will increase until above the shakedown limit multiplier, and then the iterative process continues. The described convergence procedure of the SCM for shakedown analysis is vividly depicted in Fig. 4. By doing so, the method can ensure that the load multiplier approaches to the actual shakedown limit multiplier λ_{actual} from above. Since the adopted shakedown criterion is based on the Melan's static shakedown theorem and all the conditions of the static theorem are satisfied when the iterative procedure converges, the calculated shakedown limit multiplier in this paper is a lower bound to the actual shakedown solution with the predefined tolerance *tol*3.

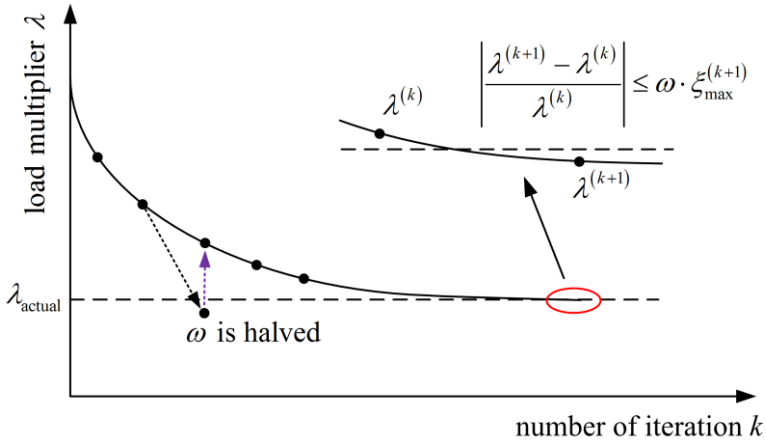

Fig. 4 Convergence procedure of the SCM for shakedown analysis

5 Numerical examples

A significant advantage of the provided method is its ability to be implemented into commercial finite element software that have the facility to allow the users to establish finite element models easily and conveniently. The described numerical algorithm in Sect. 4 has been implemented into ABAQUS [63] via user subroutines UAMT and URDFIL. In order to illustrate the performance of the present algorithm, three numerical examples of limit and shakedown analysis are considered. It is mentioned here that limit analysis is considered as a special case of shakedown analysis when the number of load vertices is reduced to one.

In all examples, the materials are assumed homogeneous, isotropic and elastic-perfectly plastic with the von Mises yield criterion. All material parameters are constant over time and independent of temperature. All the calculations are carried out on the personal computer with 16 GB RAM and Intel Core i7 at 3.39 GHz using single processor.

5.1 Square plate with a circular central hole

Fig. 5 shows a square plate with a circular central hole subjected to biaxial loads P_1 and P_2, which is a common benchmark example for numerical limit and shakedown analysis [24,26,28,30,31,38,41,44,55,64-70]. The mechanical material data are given in Table 1. The ratio between the diameter D of the circular hole and the length L of the plate is 0.2. The ratio between the thickness d of the plate and its length L is 0.05.

Considering the symmetry of the structure and the loading, only one quarter model is

established for the analysis. Since the thickness d of the plate is much smaller than its length L, both a plane stress problem and a three-dimensional problem are analyzed here. The 2D and 3D finite element models of the plate are shown in Fig. 6. Four hundred 8-node quadratic plane stress elements (ABAQUS CPS8) with 3×3 Gauss integration points are used for the plane stress problem in Fig. 6(a), and twelve hundred 20-node quadratic brick elements (ABAQUS C3D20) with 3×3×3 Gauss integration points are used for the three-dimensional problem in Fig. 6(b).

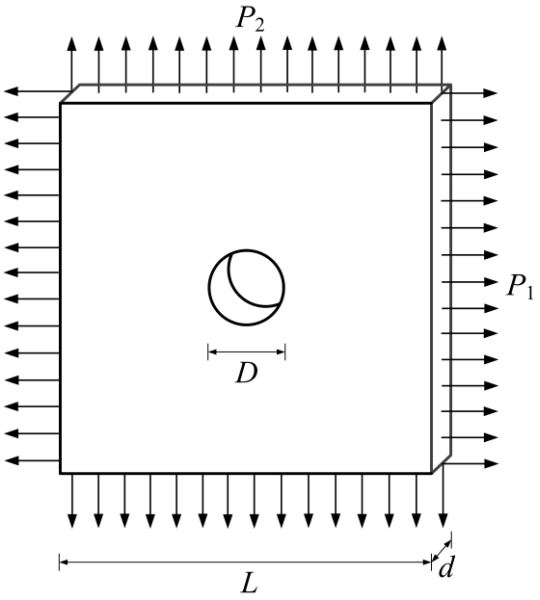

Fig. 5 Geometry of the holed plate under biaxial loading

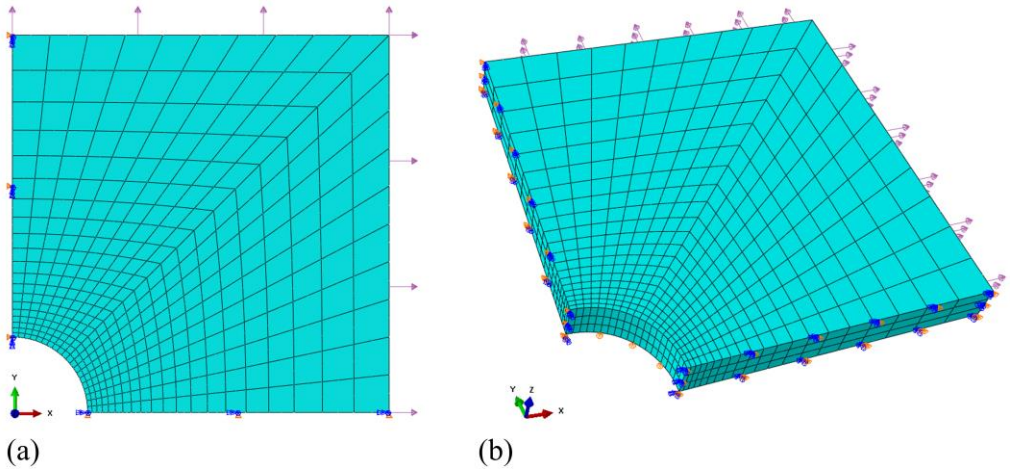

Fig. 6 Finite element models: (a) for the plane stress problem; (b) for the three-dimensional problem

Table 1 Material properties of the plate

Young's modules E (GPa)	Poisson's ratio v	Yield stress σ_y (MPa)
200	0.3	360

This benchmark problem has been studied by several authors, since it was first investigated by Belytschko [67]. Some comparative studies have been presented in their literatures, such as [24,28,30,31,38,44,55,69,70]. As a result, there is no exact solution that is generally accepted and the shakedown load is relevant to the loading mode. So four different loading histories are considered, as illustrated in Fig. 7. For loading path a, P_1 and P_2 vary independently. For loading path b, P_1 and P_2 vary proportionally. For loading path c, P_1 keeps constant and P_2 varies from nil to a certain value. For loading path d, P_1 keeps constant and P_2 varies from minus to plus.

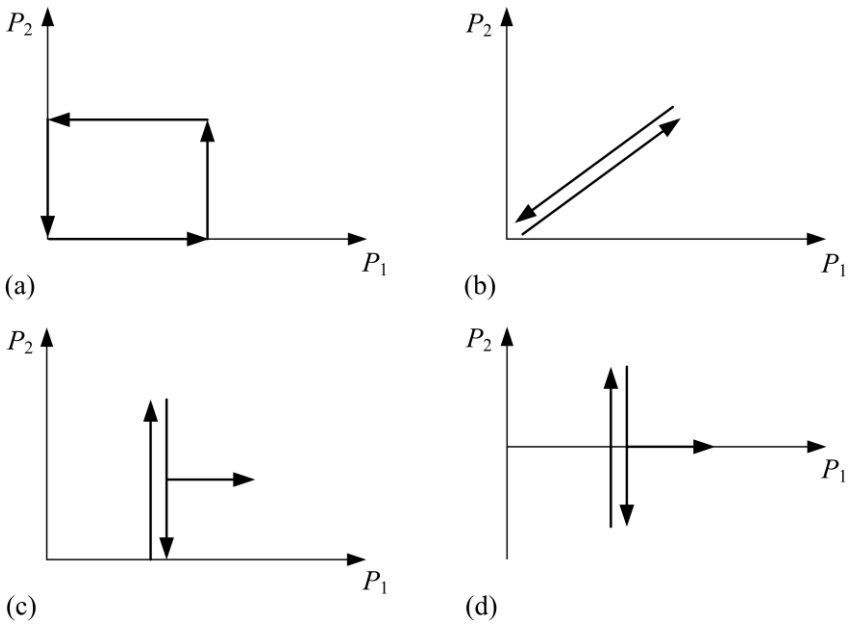

Fig. 7 Four loading histories for shakedown analysis: (a) loading path a; (b) loading path b; (c) loading path c; (d) loading path d

5.1.1 P_1 and P_2 vary independently

The plate is subjected to biaxial uniform loads P_1 and P_2 that vary independently in the following ranges:

$$\begin{aligned} 0 \le P_1 \le \mu_1 P_0 \\ 0 \le P_2 \le \mu_2 P_0 \end{aligned} \tag{35}$$

The shakedown limits calculated by the SCM are compared to the mentioned results [24,26,28,30,31,38,41,44,64-70] for the three special loading cases $\mu_2 = 0$, $\mu_2 = 0.5\mu_1$ and $\mu_2 = \mu_1$ in Table 2. The values of shakedown limits in Table 2 are normalized with the ratio P_0/σ_y. As explained in Ref. [30], the partly-analytical solution by Zhang [68] can be considered as the reference solution.

Table 2 Comparison of different numerical results for shakedown analysis

Authors and References	Loading cases		
	$\mu_2 = \mu_1$	$\mu_2 = 0.5\mu_1$	$\mu_2 = 0$
Belytschko [67]	0.431	0.501	0.571
G. Zhang [68]	0.431	0.514	0.596
Groß-Weege [69]	0.446	0.524	0.614
Carvelli et al. [64]	0.518	--	0.696
Chen and Ponter [24]	0.492	--	0.666
Chen and Ponter (3D) [24]	0.532	--	0.709
Zhang and Raad [65]	0.494	--	0.574
Zouain et al. [31]	0.429	0.500	0.594
Garcea et al. [26]	0.438	0.508	0.604
Liu et al. [38]	0.477	0.549	0.647
Akoa et al. (3D) [66]	0.466	--	0.637
Krabbenhøft et al. [70]	0.430	0.499	0.595
Chen et al. [44]	0.480	0.553	0.649
Tran et al. [41]	0.434	--	0.601
Simon and Weichert (3D) [30]	0.458	0.531	0.627
Spiliopoulos and Panagiotou [28]	0.522	--	0.700
Reference solution	0.431	0.514	0.596
Present solution (ABAQUS CPS8)	0.440	0.510	0.607
Relative error (ABAQUS CPS8)	2.09%	1.05%	1.85%
Present solution (ABAQUS C3D20)	0.434	0.504	0.600
Relative error (ABAQUS C3D20)	0.70%	2.21%	0.50%

(3D) denotes that the results are obtained from three-dimensional model, and the other results are obtained from plane stress model.

As we can see, the different numerical results in Table 2 show that our solution is in great agreement with the values from the reference solution where the maximum relative error is only 2.09% for plane stress problem and 2.21% for three-dimensional problem. It should be noted that there is a relatively large range among those numerical results. The discrepancy is attributed not only to the different methods but also to the different types of finite elements and sizes of the element meshes used for the initial elastic solution. A simple way to illustrate the influence of finite elements is the existing difference of the maximum elastic stress between in this paper and in Ref. [24] under same single loading P_1. The maximum elastic stress is $3.297P_1$ when the finite element meshes in this paper are used but is $2.891P_1$ when the element meshes in Ref. [24] are used. What's more, the maximum relative error is only 0.49% between the present solution for plane stress problem and the solution by Garcea [26], whose finite element model has the most approximate mesh size with the finite element model in Fig. 6(a).

After calculating the shakedown limits for various ratios of μ_1/μ_2 by using the SCM, the shakedown domain was obtained. As illustrated in Fig. 8, these points of shakedown limits align in two straight-line segments and the results coincide well with the reference solution. Furthermore, the shakedown boundary in Fig. 8 is dominated by alternating plasticity.

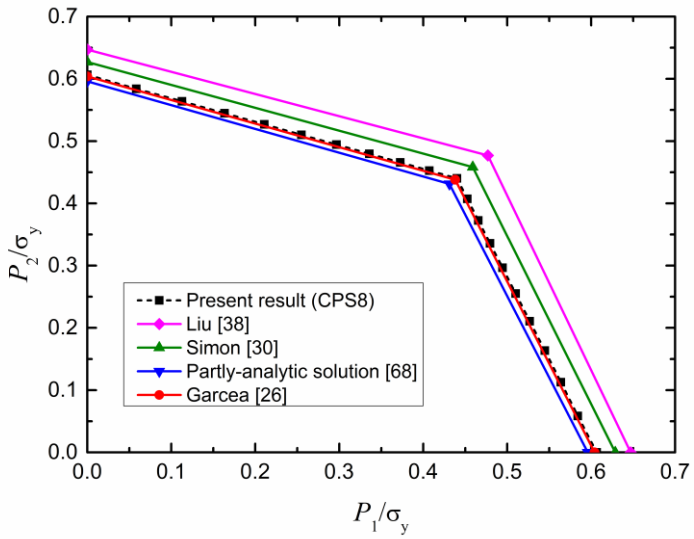

Fig. 8 Shakedown domains of the square plate for loading path a

Fig. 9 shows the typical convergence procedure of shakedown analysis for the holed plate

under loading case $\mu_2 = 0$. The horizontal line segment in the Fig. 9 indicates that the procedure is being carried out for the steady cyclic state, and the decreasing values indicate the procedure is being carried out for the iterative process of the load multipliers. Although, with the increase of iteration number, the calculated load multipliers do not strictly decrease monotonically, the solutions converge to the stable one which is the actual solution with a specified tolerance (10^{-4}) by using the reasonable iterative control technique.

The crucial idea of the Melan's theorem for shakedown analysis is to find an optimal time-independent self-equilibrated residual stress field. As a result, a final residual stress field of the holed plate is shown in Fig. 10. It should be noted that, the calculated residual stress field by the SCM is non-unique and related to the initial load multiplier, but the calculated shakedown limit multipliers are the same for different initial load multipliers, which verifies the discussions in Sect. 2.3.

In order to illustrate the efficiency of the proposed procedure for shakedown analysis, the computing time for some cases with different number of finite elements is compared in Table 3. For the finite element model with 400 8-node quadratic plane stress elements in Fig. 6(a), the amount of CPU time ranges from 6 s for the case of $\mu_2 = 0$ to 11 s for $\mu_2 = \mu_1$. Specially, for a large-scale three-dimensional finite element problem with 20000 20-node quadratic brick elements (ABAQUS C3D20), the computing time is only 2558 s.

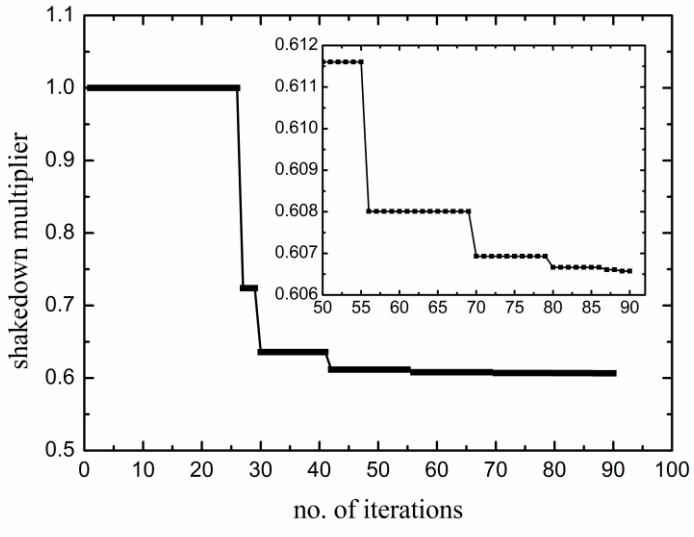

Fig. 9 Convergence procedure of the SCM for loading case a ($\mu_2 = 0$)

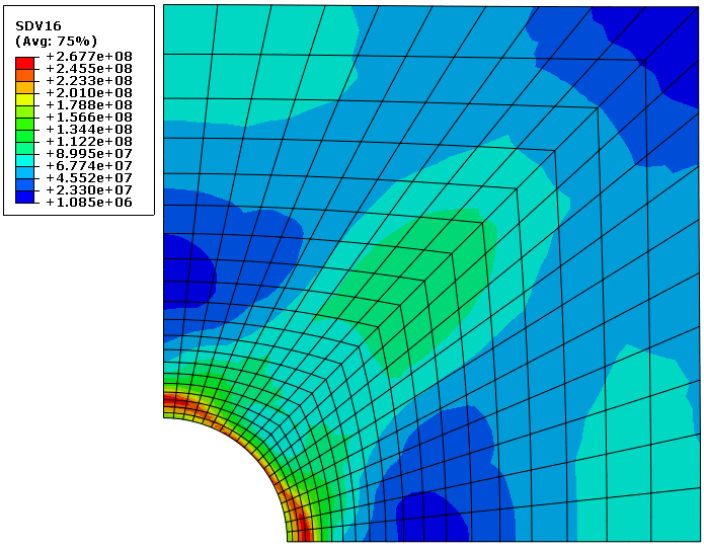

Fig. 10 Equivalent residual stress field of the holed plate for loading case a ($\mu_2 = 0$)

Table 3 Computing time for shakedown analysis of the holed plate

Finite Elements	Loading cases	μ_1	μ_2	CPU time (s)
400 CPS8	$\mu_2 = 0$	0.607	0	6
400 CPS8	$\mu_1 = \mu_2$	0.440	0.440	11
400 CPS8	$\mu_1 = 1.25\mu_2$	0.466	0.373	10
1200 C3D20	$\mu_1 = \mu_2$	0.434	0.434	131
20000 C3D20	$\mu_1 = \mu_2$	0.429	0.429	2558

5.1.2 P_1 and P_2 vary proportionally

The shakedown analysis of the holed plate with P_1 and P_2 varying proportionally is also considered by using the SCM. The same case has already been analyzed by some authors [26,28,53] and the present results are compared in Fig. 11. It is worth noting that, for the present results in Fig. 11, the straight-line portion of the shakedown boundary curve is dominated by alternating plasticity, and the rest portion of the curve is due to the plastic collapse.

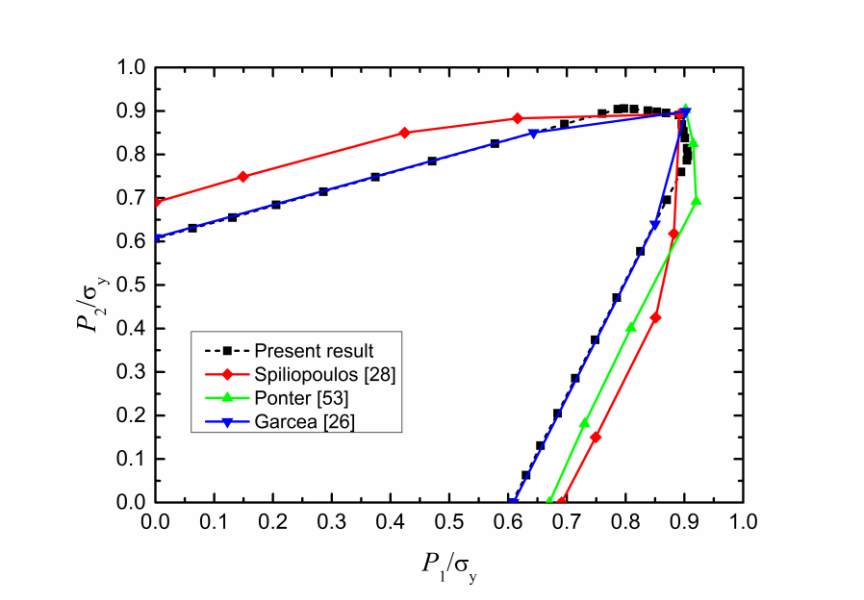

Fig. 11 Shakedown domain of the square plate for loading path b

5.1.3 P_1 is constant and P_2 is cyclic

The SCM is used to calculate the shakedown limits of the plate under loading path c and loading path d (Fig. 7). These two shakedown problems have been considered by Chen and Ponter [55]. In order to exclude the discrepancy of the mesh discretization, the comparison of the calculated results by the SCM and those by the LMM is based on the same finite element model. Fig. 12 and Fig. 13 give the shakedown domains of the square plate under loading path c and loading path d, respectively. Each figure of them includes the shakedown domains by the SCM with two different kinds of mesh discretization, the shakedown domain by the LMM, and the results from Ref. [55]. The mark “mesh 1” in the legend denotes that the mesh displayed in Fig. 6(a) is used, and the mark “mesh 2” denotes that the mesh from Ref. [55] is used.

We can observe from Fig. 12 and Fig. 13 that the results obtained by the SCM and the LMM agree very well with each other for the same mesh model, which verifies the validity of the two methods. Nevertheless, for the different mesh models, there are obvious differences in the plateaus of shakedown boundary curves, while the rest of the curves are very agreeable. The differences are in fact due to the different failure modes of the structure. In both Fig. 12 and Fig. 13, the plateau portions of these shakedown boundary curves are dominated by

alternating plasticity, for which the shakedown limit is relevant to the local maximum stress. Thus, the difference in the local maximum stress due to the inconsistent mesh leads to the different shakedown limits. However, if the structure fails due to incremental plasticity, as is the rest portion of these shakedown boundary curves in Fig. 12 and Fig. 13, the shakedown limit is insensitive to the mesh.

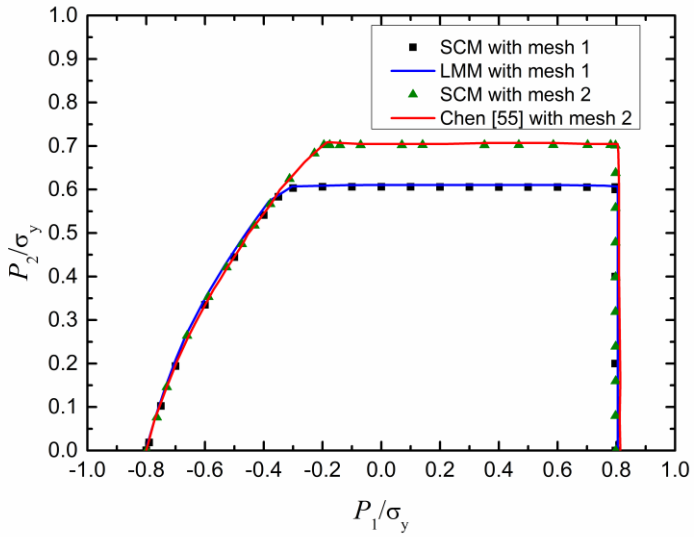

Fig. 12 Shakedown domains of the square plate for loading path c

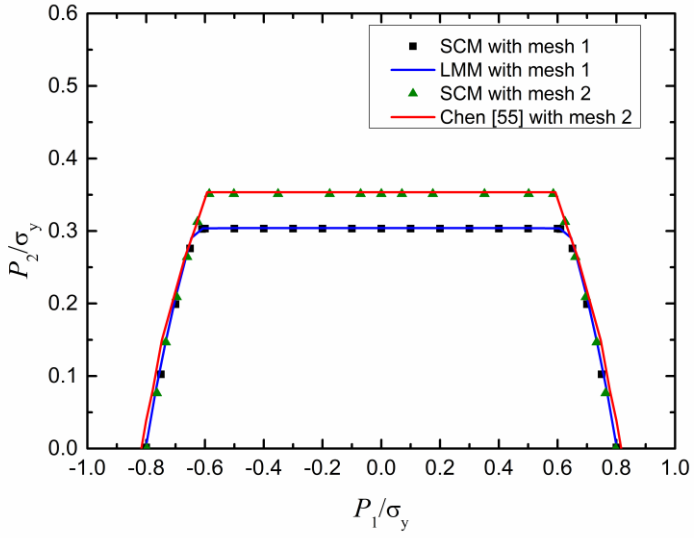

Fig. 13 Shakedown domains of the square plate for loading path d

In the above examples, the shakedown domains are all obtained by the SCM under different loading paths. The present results by the proposed method are all in agreement with

those by other methods.

5.2 Defective pipeline

Pipelines, which are generally made up of ductile steel, are widely used in various fields, such as petrochemical industry, energy, nuclear industry, and electric power engineering, etc. During their operation, many defects such as part-through slots can be produced by mechanical damage, corrosion or abrading surface cracks. These defects may jeopardize the integrity (i.e. reduce the load-carrying capacity) of pipelines and sometimes even lead to severe industrial accidents. The integrity assessment of pipelines with part-through slots is a very important research subject with significant and extensive application background in the industry. Plastic limit and shakedown analysis plays a significant role in the integrity assessment of defective pipelines. In this paper, through some computational examples and analyses, the effects of small and large area slots on the load-carrying capacity of pipelines are investigated and evaluated.

These examples adopted here are three-dimensional defective pipelines under internal pressure and axial tension [24]. The geometry of the structure is shown in Fig. 14. The mechanical material data are given in Table 4. It should be noted that the applied total axial loads consist of the independent axial tension N and the additional axial tension N_1 induced by independent internal pressure P. The additional axial tension N_1 is equal to $P\pi R_i^2$, where R_i is the inner radius of pipeline. Here a small spherical slot and a large area slot are considered for limit and shakedown analyses. The geometric parameters of the slotted pipelines are presented in Table 5.

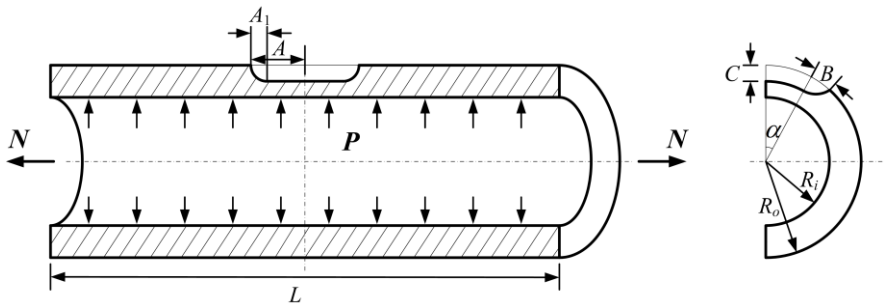

Fig. 14 Geometry of pipeline with part-through slot subjected to internal pressure and axial tension

Table 4 Material properties of pipelines

Young's modules E (GPa)	Poisson's ratio v	Yield stress σ_y (MPa)
200	0.3	245

Table 5 Geometric parameters of pipelines with different defect types (mm)

Defect type	R_i	R_o	L	α	A_1	A	B	C
Small slot	17	21	250	0	2	2	2	2
Large area slot	17	21	250	45°	2	10	2	2

Due to the symmetry of the structure and the loading, only a quarter of the defective pipeline is considered. The corresponding displacement constraints are imposed on the symmetric boundaries. The 3D finite element mesh discretization of the pipeline is shown in Fig. 15, where the 20-node quadratic brick elements (ABAQUS C3D20) with 3×3×3 Gauss integration points are used. In order to optimize the efficiency and accuracy of the calculation, the finite elements around the slots should be distributed appropriately to make them as much neat and fine as possible. The numbers of finite elements used to discretize the pipelines with a small slot and with a large area slot are 1905 and 1658, respectively.

The SCM is used to calculate the shakedown limits of the defective pipeline under axial tension and internal pressure with five different loading paths, as shown in Fig. 16. For loading path a, the single load N varies from nil to a certain value. For loading path b, the single load P varies from nil to a certain value. For loading path c, three vertices of the loading path are included, in which the maximum independent axial tension N (replaced by the equivalent uniform tension) is four times of the maximum internal pressure P. For loading paths d and e, the single load N and P keep certain value, respectively. The loading paths d and e are used to calculate the limit loads of the defective pipeline subjected to independent axial tension and internal pressure, respectively.

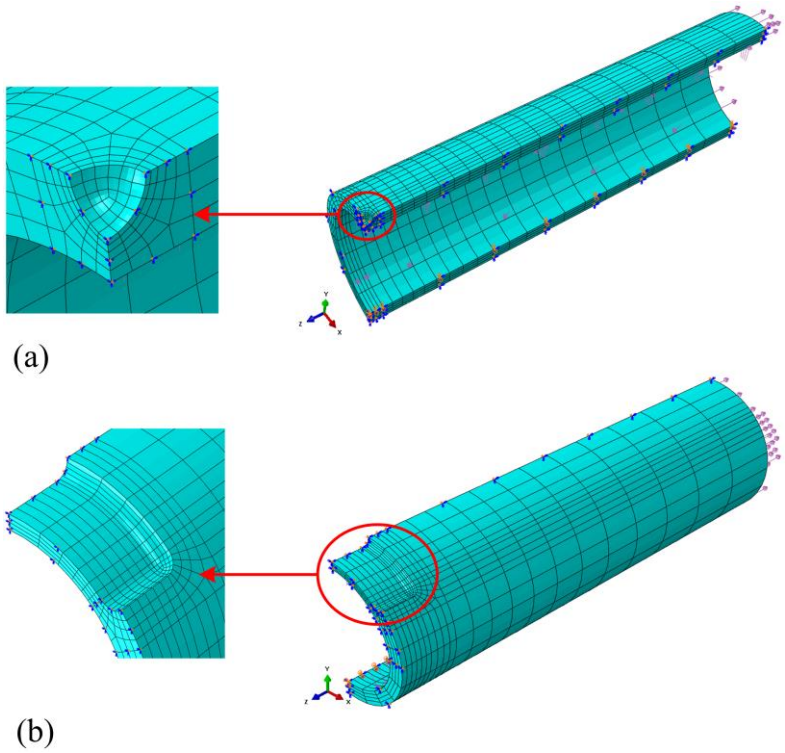

Fig. 15 3D finite element meshes for slotted pipeline: (a) with a small slot; (b) with a large area slot

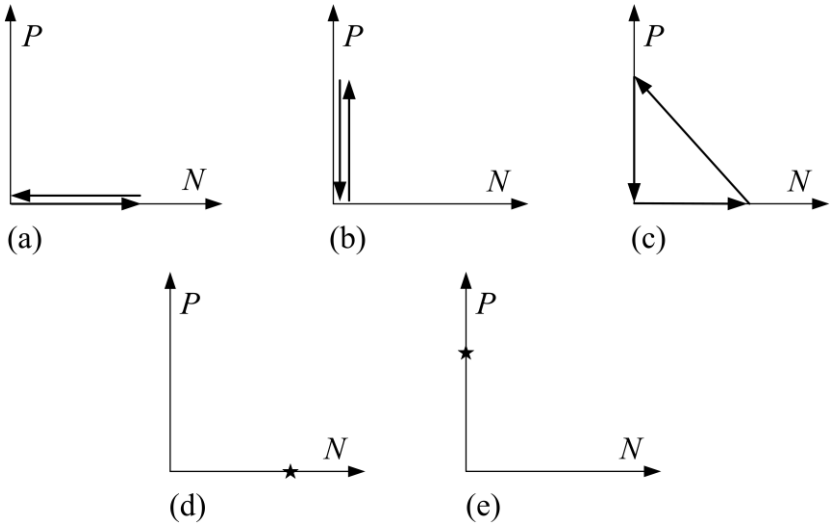

Fig. 16 Five different loading paths for shakedown analyses

As we all know, the shakedown limit of elastoplastic structure under proportional load is the minimum one of its plastic limit load and its double elastic limit load. Thereby, the shakedown limit of the defective pipeline can be determined via an elastic-plastic incremental analysis and a linear elastic analysis using the finite element software ABAQUS.

As a powerful direct method, the liner matching method was proposed by Chen and

Ponter [24], and was used for the shakedown and limit analyses of three-dimensional structures. In this paper, the shakedown and limit loads of the defective pipelines under axial tension and internal pressure with the five loading paths shown in Fig. 16 are calculated by the above three different methods, i.e., the SCM, the method of ABAQUS and the LMM.

It should be explained that the defective pipelines considered here have the same geometry, mechanical material data and load conditions as those in Ref. [24], but are different in mesh discretization with the reference. In order to compare the performance of the SCM and the LMM reasonably, the same finite element model must be considered. The present numerical results by the LMM for defective pipelines are based on the finite element models in Fig. 15, which has a slight difference with the results in Ref. [24].

Table 6 and Table 7 show the numerical results of shakedown analysis for the pipelines with a small slot and with a large area slot, respectively. It can be seen that the shakedown limits obtained by the SCM are in excellent agreement with the solutions by the method of ABAQUS and the LMM. As a general result, the linear matching method is an upper bound method, by which the calculated shakedown loads are bigger than that by the other two methods. For the pipeline with a large area slot under the five different loading histories, the maximum deviation of the shakedown loads between the results calculated by the SCM and that by the method of ABAQUS is 2.9%.

Table 6 Shakedown limit for the pipeline with a small slot under five different loading paths using three different methods

Loading paths	Shakedown limit (MPa) for the load domain		
	SCM	ABAQUS	LMM
Case a	(0,0), (229.6,0)	(0,0), (229.8,0) [1]	(0,0), (229.7,0)
Case b	(0,0), (0,56.8)	(0,0), (0,57.0) [1]	(0,0), (0,57.1)
Case c	(0,0), (172.0,0), (0,43.0)	---	(0,0), (173.3,0), (0,43.32)
Case d	(0,0), (242.1,0)	(0,0), (244.5,0)	(0,0), (244.8,0)
Case e	(0,0), (0,57.4)	(0,0), (59.1,0)	(0,0), (0,59.7)

( ) [1], the superscript indicates the shakedown load is determined by the double elastic limit load.

( ) [2], the superscript indicates the shakedown load is determined by the plastic limit load.

Table 7 Shakedown limit for the pipeline with a large area slot under five different loading paths using three different methods

Loading paths	Shakedown limit (MPa) for the load domain		
	SCM	ABAQUS	LMM
Case a	(0,0), (168.7,0)	(0,0), (168.7,0) [1]	(0,0), (169.9,0)
Case b	(0,0), (0,38.4)	(0,0), (0,39.3) [2]	(0,0), (0,39.5)
Case c	(0,0), (142.8,0), (0,35.7)	---	(0,0), (143.8,0), (0,35.9)
Case d	(0,0), (208.2,0)	(0,0), (212.6,0)	(0,0), (215.3,0)
Case e	(0,0), (0,38.7)	(0,0), (0,39.3)	(0,0), (0,39.5)

( ) [1], the superscript indicates the shakedown load is determined by the double elastic limit load.

( ) [2], the superscript indicates the shakedown load is determined by the plastic limit load.

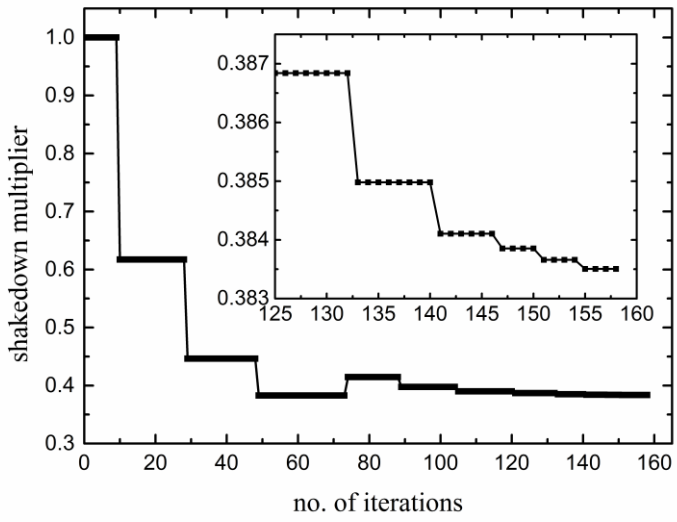

Fig. 17 Convergence procedure of the SCM towards the shakedown load for the defective pipeline with a large area slot under loading case b

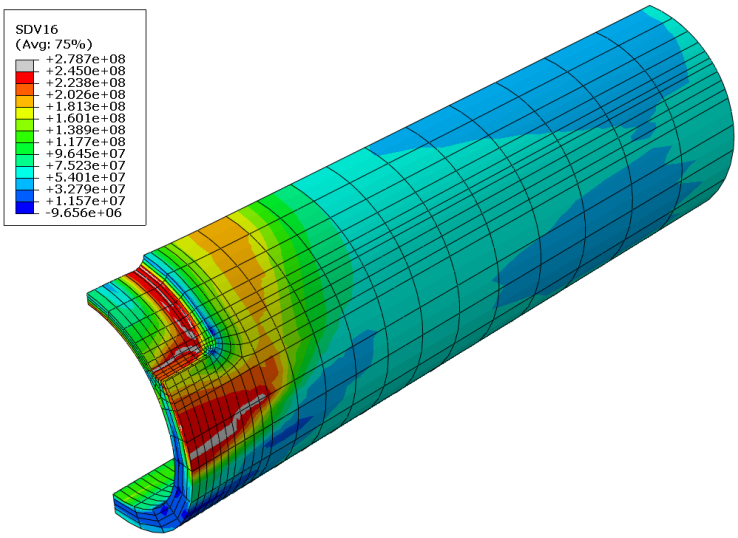

Fig. 18 Equivalent residual stress field of the defective pipeline with a large area slot under loading case b

Under the proposed five loading paths, all the calculations for shakedown analysis of these defective pipelines have good convergence condition. As an example, the convergence procedure of the SCM towards the shakedown load for the defective pipeline with a large area slot under loading path b is shown in Fig. 17. Moreover, this case generates the maximum number of iteration for the five cases considered here. It should be noted that the increase of the shakedown multiplier during the process of the iteration indicates that an overshooting of the shakedown limit has occurred in the previous iteration. However, the shakedown multiplier still converges to the final result by halving the convergence parameter ω. The final equivalent residual stress field is shown in Fig. 18.

Assuming the axial tension and internal pressure vary independently, the SCM is used to calculate the shakedown limits of the pipeline for various ratios of the applied axial tension and internal pressure. Then shakedown domains of the defect-free pipeline as well as the defective pipelines with a small slot and with a large area slot are presented in Fig. 19.

In order to demonstrate the computational efficiency of the SCM for complex three-dimensional problem, the LMM and the step-by-step procedure are also used to calculate the shakedown load of the pipeline for same ratios of the applied axial tension and internal pressure. Without loss of generality, five load domains are considered and the corresponding computed results are displayed in Fig. 19 additionally. The CPU times for

shakedown analysis of the defective pipelines under three load domains by the SCM, the LMM and the step-by-step procedure are compared in Table 8. It can be seen from Table 8 that, with necessary accuracy of calculations (see Fig. 19), the CPU time by the step-by-step procedure is 20 times more than that by the SCM while the computational efficiency of the SCM is higher than that of the LMM.

As a by-product, the strain history of the pipeline under cyclic loading is also obtained from the incremental elastic-plastic calculation. In Fig. 19, the load conditions marked with capital letters “A” and “B” are acted on the defective pipelines with a small slot while the load conditions marked with capital letters “C” and “D” are acted on the defective pipelines with a large area slot. Fig. 20 shows the effective plastic strains of the pipeline with a small slot over the first 10 load cycles for point “A” and point “B”. It can be seen that the pipeline with a small slot exhibits alternating plasticity behavior for point “A” and shakedown behavior for point “B”. Fig. 21 shows the effective plastic strains of the pipeline with a large area slot over the first 15 load cycles for point “C” and point “D”. The pipeline with a large area slot shakes down after 11 load cycles for point “D”, but failures due to the incremental plasticity mechanism for point “C”.

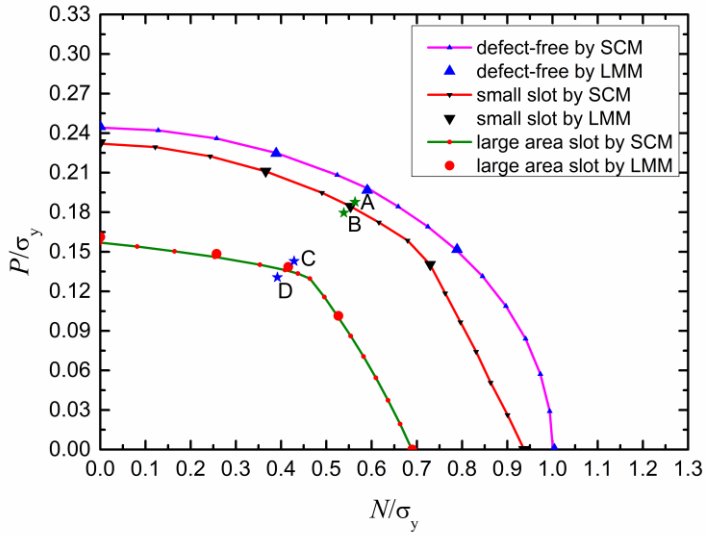

Fig. 19 Shakedown domains of the defect-free pipeline and the defective pipelines with a small slot and with a large area slot

Table 8 CPU time (s) for shakedown analysis of the defective pipeline under different load domains by the SCM, the LMM and the step-by-step procedure

Load domains (MPa) $0 \le N \le 300\sin\theta$ $0 \le P \le 100\cos\theta$	With a small slot			With a large area slot		
	SCM	LMM	Step-by-step	SCM	LMM	Step-by-step
$\theta = 30^{\circ}$	324	660	6211	319	480	6735
$\theta = 45^{\circ}$	291	635	5984	303	493	6612
$\theta = 60^{\circ}$	325	611	6121	311	562	6786

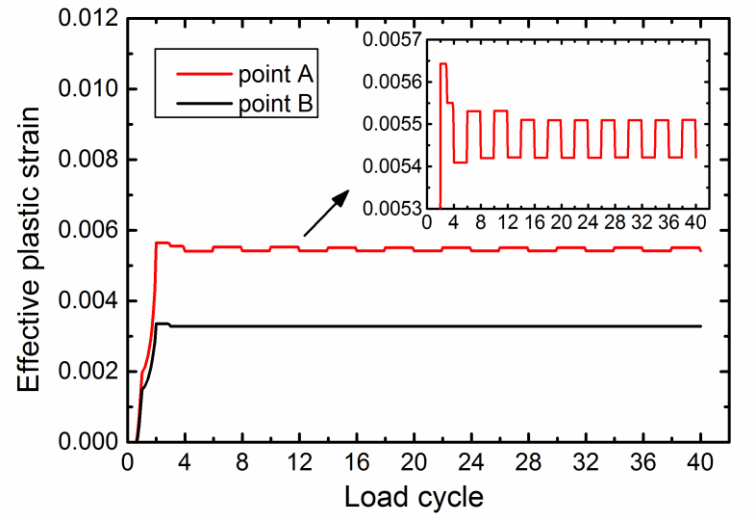

Fig. 20 Effective plastic strains of the pipeline with a small slot over the first 10 load cycles for point “A” and point “B”

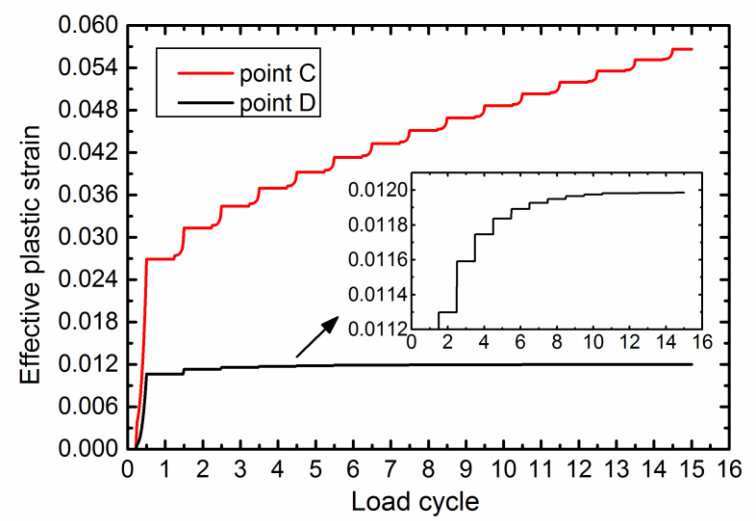

Fig. 21 Effective plastic strains of the pipeline with a large area slot over the first 15 load cycles for point “C” and point “D”

5.3 Header component

The third numerical example is a header component, which is typically used in an advanced gas-cooled reactor (AGR) power plant. In the cooling and reheating process of the AGR, the header often experiences complex load conditions due to its interaction with the rest of the piping system. Here, a schematic of the header component is shown in Fig. 22, where the main pipe has two vertical branch pipes with the same geometric dimension. In the present paper, some typical loading cases are considered and the shakedown boundaries of the header component under different load domains are calculated by the SCM.

The header component is depicted by some characteristic dimensions in Fig. 22, and the values of these dimensions are listed in Table 9. For the convenience of calculation, the material properties are assumed constant over time and independent of temperature. The detailed mechanical material data of the header component are given in Table 10.

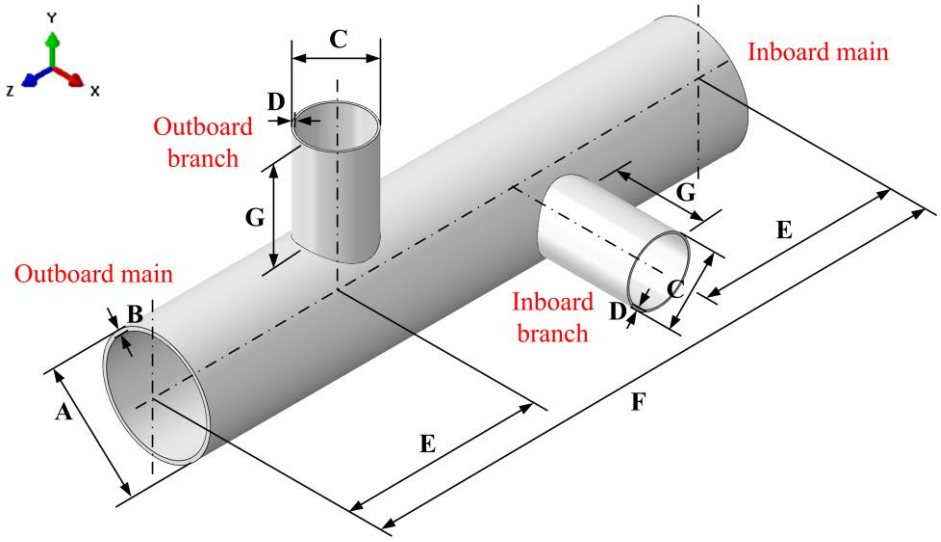

Fig. 22 Geometry of the header component

Table 9 Geometric parameters of the header component (mm)

Dimension	A	B	C	D	E	F	G
Value	600	20	350	10	1000	3000	500

Table 10 Material properties of the header component

Young's modules E (GPa)	Poisson's ratio v	Yield stress σ_y (MPa)
200	0.3	165

Three groups of different loads are applied to the header component, whose fundamental loads are listed in Table 11. For the first group, the internal pressure $P_i = 3.64\,\text{MPa}$ is applied to all internal surfaces of the structure, and the internal pressure leads to additional tensions at ends of the main and branch pipes. For the second group, the axil force F, which has been replaced by the equivalent uniform pressure $P_F = 40\,\text{MPa}$, is applied to the outboard main pipe end. For the third group, the bending moment $M_{mx} = 240\,\text{kN}\cdot\text{m}$ and $M_{my} = -160\,\text{kN}\cdot\text{m}$ are applied to the outboard main pipe end, and the bending moment $M_{bz} = -9.6\,\text{kN}\cdot\text{m}$ is applied to the inboard branch pipe end. It should be noted that these three bending moments are assumed to vary synchronously. Hence, the amplitudes of the three group loads can be determined by three dimensionless load factors, i.e. P_0, F_0 and M_0.

In order to balance the efficiency and accuracy of the calculation, the 20-node quadratic brick elements with reduced integration (ABAQUS C3D20R) are used to discretize the structure, and the meshes around the area of stress concentration are refined properly. As shown in Fig. 23, the mesh discretization consists of 27540 elements and 139251 nodes. The reference points and kinematic coupling constraints are used to apply the bending moments and boundary conditions to the model.

Table 11 Fundamental loads applied to the header component

Load	P_0			F_0	M_0		
	Internal pressure P_i (MPa)	Main tension P_{ma} (MPa)	Branch tension P_{br} (MPa)	P_F (MPa)	M_{mx} ($\text{kN}\cdot\text{m}$)	M_{my} ($\text{kN}\cdot\text{m}$)	M_{bz} ($\text{kN}\cdot\text{m}$)
Value	3.64	-24.60	-29.15	40	240	-160	-9.6

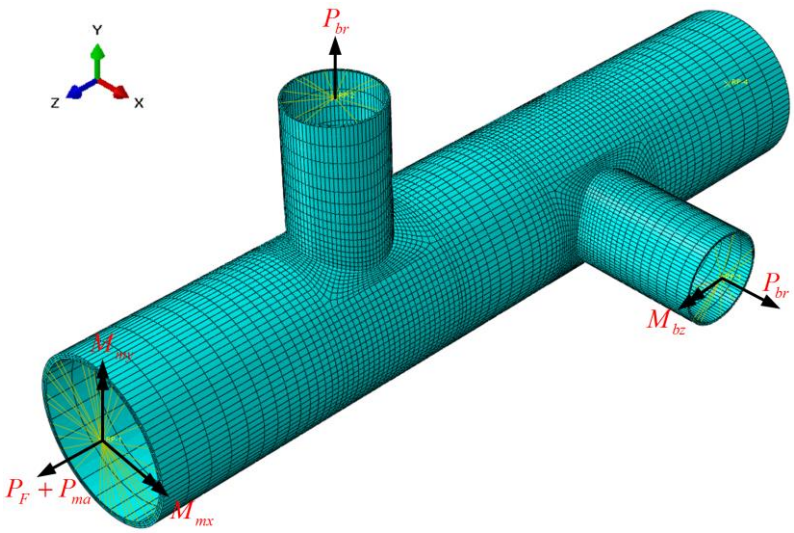

Fig. 23 Finite element model of the header component

Here, two types of combinations of two loadings are considered.

(1) Combination I

We consider the load factor F_0 equals to zero, and then the load domains of interest are dominated by the load factor P_0 and M_0, as displayed in Fig. 24.

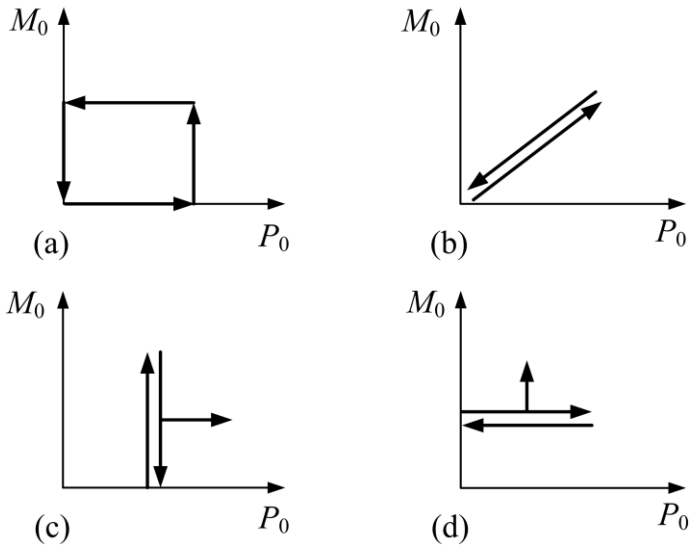

Fig. 24 Four different load domains for combination I: (a) domain a; (b) domain b; (c) domain c; (d) domain d

The SCM is used to calculate the shakedown limits of the header component for various loading cases. As results, four shakedown boundaries corresponding to the four load domains are presented in Fig. 25. For the load domains a and b, alternating plasticity is the critical failure mode. However, for the load domains c and d, the critical failure mode consists of

alternating plasticity (curve 1 and curve 4 in Fig. 25) and incremental plasticity (curve 2 and curve 3 in Fig. 25). It should be noted that the load history is dominated by one parameter in the load domain b, thus, the shakedown load is the double elastic limit load. For comparison, the elastic boundary is also presented in Fig. 25. The shakedown boundary curve for the load domain b has the same shape and twice values in amplitude as the elastic boundary curve.

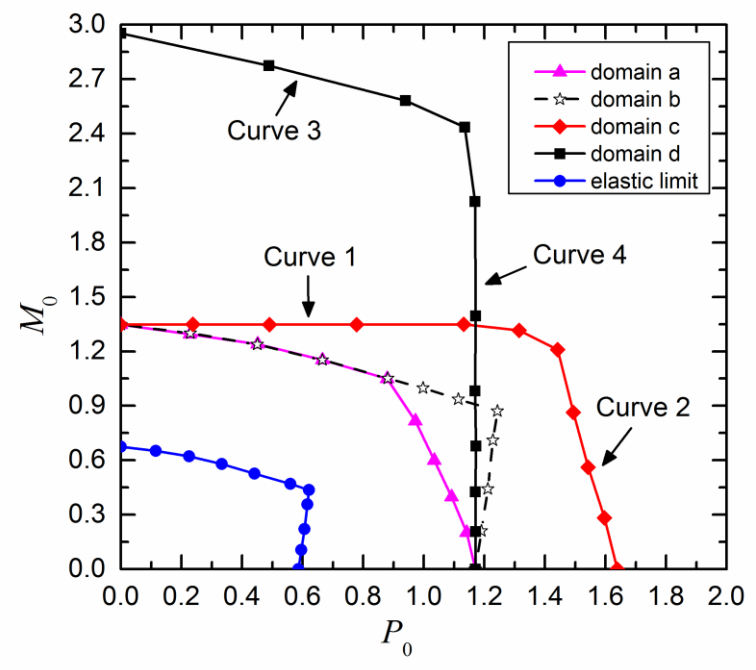

Fig. 25 Shakedown domains of the header component for combination I: P_0 versus M_0

(2) Combination II

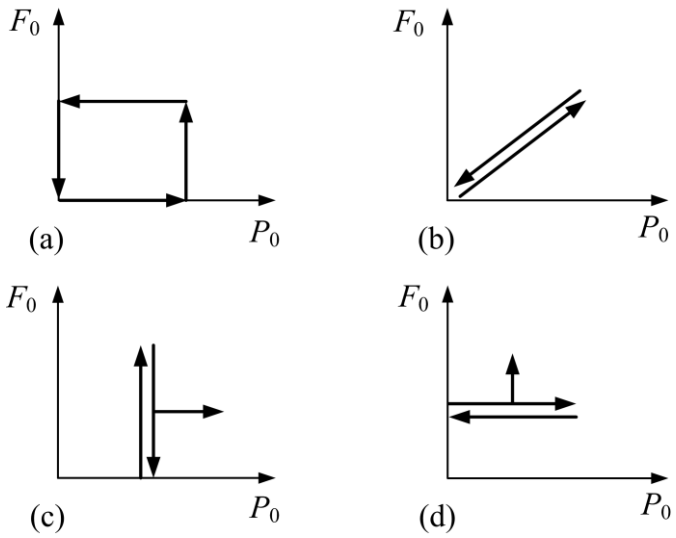

Fig. 26 Four different load domains for combination II: (a) domain a; (b) domain b; (c) domain c; (d) domain d

Here, we consider that the load factor M_0 equals to zero. The load domains of interest are dominated by the load factor P_0 and F_0, as displayed in Fig. 26.

The SCM is used to calculate the shakedown limits of the header component. Four shakedown boundaries corresponding to the four load domains and the elastic boundary are all presented in Fig. 27. It is obvious that the shapes of the four calculated shakedown boundaries for the combination II are very similar to these for the combination I. Furthermore, the same critical failure modes dominating the shakedown boundaries are observed for the two types of load combinations.

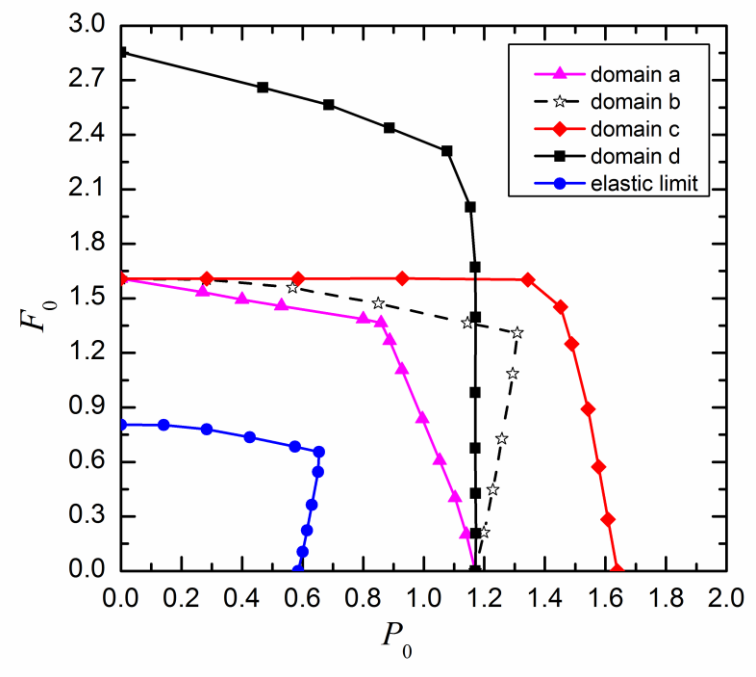

Fig. 27 Shakedown domains of the header component for combination II: P_0 versus F_0

To the authors' best knowledge from literatures, until now, the shakedown problem of this comparable scale has never been solved before. In this paper, about one hundred calculations have been completed to demonstrate the performance of the SCM for shakedown analysis of the large-scale header component under various load conditions. All iterative procedures of the SCM for shakedown analysis present good convergence. The convergence tolerances are all met within 270 increments, and the CPU time is not more than 40 minutes. The equivalent residual stress field of the header component is also obtained conveniently, as shown in Fig. 28.

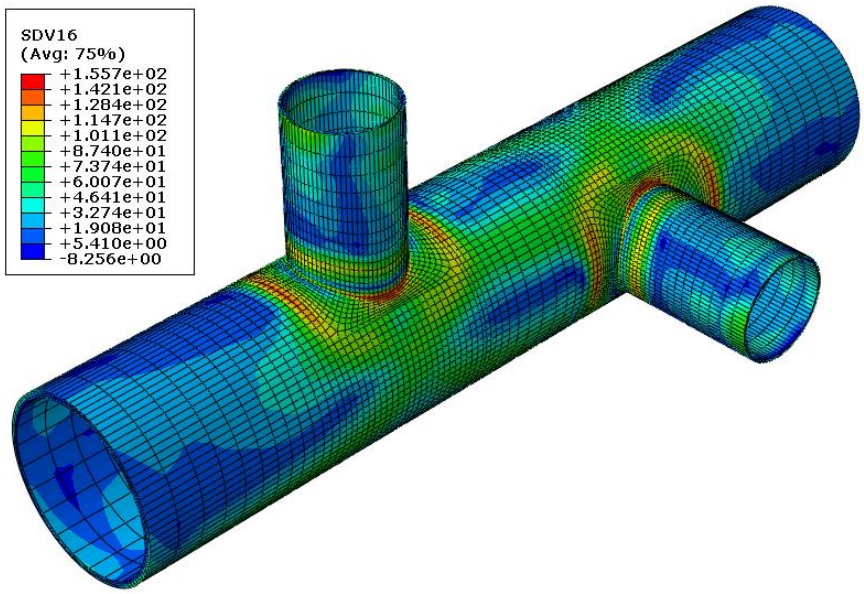

Fig. 28 Equivalent residual stress field of the header component

6 Discussion and conclusions

A novel direct method so-called the stress compensation method (SCM) for the application of limit and shakedown analysis to large-scale elastoplastic structures has been proposed, where a two-level iterative procedure is performed by a series of linear elastic finite element analyses and the conventional mathematical programming problem does not need to be solved. The global stiffness matrix is decomposed only once during the whole procedure, which contributes to the high efficiency of the SCM, especially for large-scale problems. By adopting an efficient and robust iteration control technique, the convergence and the accuracy of the SCM are ensured. Since all the conditions of the static shakedown theorem can be satisfied when the iterative process converges, the shakedown limit calculated by the SCM is a lower bound approximate to the actual solution with predefined tolerance.

Comparing the SCM with the residual stress decomposition method for shakedown (RSDM-S) [28], one may note that the RSDM-S decomposes the residual stresses into Fourier series with respect to time and thus requires many time points inside the cycle to represent the applied loading. After each iteration of the numerical procedure, these Fourier coefficients need to be calculated at all Gauss points by performing the numerical integration of residual stress rate over all time points of the cycle. The RSDM-S is suitable to solve shakedown problem of 2D structures at present. However, the SCM makes full use of the basics of

shakedown theory. The residual stresses are just directly calculated in a relatively small number of load vertices of a loading history and the novel iteration control technique is adopted to speed up the convergence, which improves greatly the computational efficiency of the SCM. The calculation scheme of load multiplier makes the SCM capable of solving effectively shakedown problems of complex 2D and 3D engineering structures.

The SCM has been well implemented into the commercial finite element software ABAQUS and then becomes a general-purpose computational tool for complex engineering structures. Three 2D and 3D numerical examples considering various loading paths are presented to demonstrate the performance of the SCM. The iterative procedures of the numerical examples all present good convergence. All the results of examples are in good agreement with the analytical solutions and the results from different numerical methods or in literatures. The direct comparison of CPU time for same shakedown analysis under the same computing environment shows that the SCM presents more than 20 times the computational efficiency of the step-by-step procedure. The SCM proves to be numerically stable, very efficient and highly accurate, and is well suitable for shakedown analysis of large-scale engineering structures.

Although the current calculations are restricted to structures with elastic-perfectly plastic material of von Mises yield surface under mechanical loading, the extensions to other structures that consider the material hardening and temperature-dependent material property under thermomechanical loading are in progress, and the results will be presented in forthcoming works.

Acknowledgments The authors would like to thank the support of the National Natural Science Foundation for Distinguished Young Scholars of China (Grant No.11325211), the National Natural Science Foundation of China (Grant No.11672147) and the Project of International Cooperation and Exchange NSFC (Grant No. 11511130057) during the course of this work.

References

1. König JA, Maier G (1981) Shakedown analysis of elastoplastic structures: a review of recent developments. Nucl Eng Des 66 (1):81-95

2. Maier G (2001) On some issues in shakedown analysis. J Appl Mech-T Asme 68 (5):799-807. doi:10.1115/1.1379368
3. Melan E (1938) Zur Plastizität des räumlichen Kontinuums. Ingenieur-Archiv 9 (2):116-126
4. Koiter WT (1960) General theorems for elastic-plastic solids. In: Sneddon, JN, Hill, R (eds) Progress in Solid Mechanics, vol 1. North-Holland: Amsterdam, pp 167-221
5. König JA (1987) Shakedown of elastic-plastic structures. Elsevier, Amsterdam
6. Peigney M (2014) Shakedown of elastic-perfectly plastic materials with temperature-dependent elastic moduli. J Mech Phys Solids 71:112-131. doi:10.1016/j.jmps.2014.06.008
7. Zarka J, Casier J (1979) Cyclic Loading on an Elastoplastic Structure. Practical Rule, Mechanics Today, Vo 6, Ed Nemet-Nasser, S, Pergamon Press
8. Zarka J (1980) Direct analysis of elastic–plastic structures with 'overlay' materials during cyclic loading. Int J Numer Meth Eng 15 (2):225-235. doi:10.1002/nme.1620150206
9. Stein E, Zhang GB, Konig JA (1992) Shakedown with Nonlinear Strain-Hardening Including Structural Computation Using Finite-Element Method. Int J Plasticity 8 (1):1-31
10. Pycko S, Maier G (1995) Shakedown theorems for some classes of nonassociative hardening elastic-plastic material models. Int J Plasticity 11 (4):367-395. doi:http://dx.doi.org/10.1016/S0749-6419(95)00004-6
11. Chinh PD (2007) Shakedown theory for elastic plastic kinematic hardening bodies. Int J Plasticity 23 (7):1240-1259. doi:10.1016/j.ijplas.2006.11.003
12. Polizzotto C (2010) Shakedown analysis for a class of strengthening materials within the framework of gradient plasticity. Int J Plasticity 26 (7):1050-1069. doi:10.1016/j.ijplas.2010.01.006
13. Weichert D (1986) On the Influence of Geometrical Nonlinearities on the Shakedown of Elastic-Plastic Structures. Int J Plasticity 2 (2):135-148. doi:10.1016/0749-6419(86)90009-4
14. Gross-Weege J (1990) A unified formulation of statical shakedown criteria for geometrically nonlinear problems. Int J Plasticity 6 (4):433-447. doi:http://dx.doi.org/10.1016/0749-6419(90)90012-4
15. Corradi L, Maier G (1974) Dynamic non-shakedown theorem for elastic perfectly-plastic continua. J Mech Phys Solids 22 (5):401-413. doi:http://dx.doi.org/10.1016/0022-5096(74)90005-2
16. Borino G, Polizzotto C (1996) Dynamic shakedown of structures with variable appended masses and subjected to repeated excitations. Int J Plasticity 12 (2):215-228. doi:http://dx.doi.org/10.1016/S0749-6419(96)00004-6
17. Chen HF, Ponter ARS (2004) A simplified creep-reverse plasticity solution method for bodies subjected to cyclic loading. Eur J Mech a-Solid 23 (4):561-577. doi:10.1016/j.euromechsol.2004.04.003
18. Klebanov JM, Boyle JT (1998) Shakedown of creeping structures. Int J Solids Struct 35 (23):3121-3133. doi:10.1016/S0020-7683(97)00359-4
19. Ponter ARS (2016) Shakedown limit theorems for frictional contact on a linear elastic body. European Journal of Mechanics - A/Solids 60:17-27. doi:http://dx.doi.org/10.1016/j.euromechsol.2016.05.003
20. Borkowski A, Kleiber M (1980) On a numerical approach to shakedown analysis of structures. Comput Method Appl M 22 (1):101-119. doi:http://dx.doi.org/10.1016/0045-7825(80)90053-5
21. Zhang Y (1995) An iteration algorithm for kinematic shakedown analysis. Comput Method Appl M 127 (1–4):217-226. doi:http://dx.doi.org/10.1016/0045-7825(95)00121-6

22. Ponter ARS, Carter KF (1997) Limit state solutions, based upon linear elastic solutions with a spatially varying elastic modulus. Comput Method Appl M 140 (3-4):237-258. doi:10.1016/S0045-7825(96)01104-8
23. Ponter ARS, Carter KF (1997) Shakedown state simulation techniques based on linear elastic solutions. Comput Method Appl M 140 (3-4):259-279. doi:10.1016/S0045-7825(96)01105-X
24. Chen HF, Ponter ARS (2001) Shakedown and limit analyses for 3-D structures using the linear matching method. International Journal of Pressure Vessels and Piping 78 (6):443-451. doi:10.1016/S0308-0161(01)00052-7
25. Casciaro R, Garcea G (2002) An iterative method for shakedown analysis. Comput Method Appl M 191 (49–50):5761-5792. doi:http://dx.doi.org/10.1016/S0045-7825(02)00496-6
26. Garcea G, Armentano G, Petrolo S, Casciaro R (2005) Finite element shakedown analysis of two-dimensional structures. Int J Numer Meth Eng 63 (8):1174-1202. doi:10.1002/nme.1316
27. Spiliopoulos KV, Panagiotou KD (2012) A direct method to predict cyclic steady states of elastoplastic structures. Comput Method Appl M 223:186-198. doi:10.1016/j.cma.2012.03.004
28. Spiliopoulos KV, Panagiotou KD (2014) A Residual Stress Decomposition based Method for the Shakedown analysis of structures. Comput Method Appl M 276:410-430. doi:10.1016/j.cma.2014.03.019
29. Vu DK, Yan AM, Nguyen-Dang H (2004) A primal–dual algorithm for shakedown analysis of structures. Comput Method Appl M 193 (42–44):4663-4674. doi:http://dx.doi.org/10.1016/j.cma.2004.03.011
30. Simon JW, Weichert D (2011) Numerical lower bound shakedown analysis of engineering structures. Comput Method Appl M 200 (41–44):2828-2839. doi:http://dx.doi.org/10.1016/j.cma.2011.05.006
31. Zouain N, Borges L, Silveira JL (2002) An algorithm for shakedown analysis with nonlinear yield functions. Comput Method Appl M 191 (23-24):2463-2481. doi:10.1016/S0045-7825(01)00374-7
32. Christiansen E, Andersen KD (1999) Computation of collapse states with von Mises type yield condition. Int J Numer Meth Eng 46 (8):1185-1202
33. Makrodimopoulos A, Martin CM (2006) Lower bound limit analysis of cohesive-frictional materials using second-order cone programming. Int J Numer Meth Eng 66 (4):604-634. doi:10.1002/nme.1567
34. Krabbenhoft K, Lyamin AV, Sloan SW (2007) Shakedown of a cohesive-frictional half-space subjected to rolling and sliding contact. Int J Solids Struct 44 (11-12):3998-4008. doi:10.1016/j.ijsolstr.2006.11.001
35. Nguyen AD, Hachemi A, Weichert D (2008) Application of the interior-point method to shakedown analysis of pavements. Int J Numer Meth Eng 75 (4):414-439. doi:10.1002/nme.2256
36. Garcea G, Leonetti L (2011) A unified mathematical programming formulation of strain driven and interior point algorithms for shakedown and limit analysis. Int J Numer Meth Eng 88 (11):1085-1111. doi:10.1002/nme.3188
37. Simon JW, Weichert D (2012) Shakedown analysis with multidimensional loading spaces. Comput Mech 49 (4):477-485. doi:10.1007/s00466-011-0656-8
38. Liu YH, Zhang XF, Cen ZZ (2005) Lower bound shakedown analysis by the symmetric Galerkin boundary element method. Int J Plasticity 21 (1):21-42. doi:10.1016/j.ijplas.2004.01.003
39. Ribeiro TSA, Beer G, Duenser C (2008) Efficient elastoplastic analysis with the boundary element method. Comput Mech 41 (5):715-732. doi:10.1007/s00466-007-0227-1

40. Le CV, Nguyen-Xuan H, Askes H, Bordas SPA, Rabczuk T, Nguyen-Vinh H (2010) A cell-based smoothed finite element method for kinematic limit analysis. Int J Numer Meth Eng 83 (12):1651-1674. doi:10.1002/nme.2897
41. Tran TN, Liu GR, Nguyen-Xuan H, Nguyen-Thoi T (2010) An edge-based smoothed finite element method for primal–dual shakedown analysis of structures. Int J Numer Meth Eng 82 (7):917-938. doi:10.1002/nme.2804
42. Nguyen-Xuan H, Rabczuk T, Nguyen-Thoi T, Tran TN, Nguyen-Thanh N (2012) Computation of limit and shakedown loads using a node-based smoothed finite element method. Int J Numer Meth Eng 90 (3):287-310. doi:10.1002/nme.3317
43. Nguyen-Xuan H, Liu GR (2015) An edge-based finite element method (ES-FEM) with adaptive scaled-bubble functions for plane strain limit analysis. Comput Method Appl M 285:877-905. doi:https://doi.org/10.1016/j.cma.2014.12.014
44. Chen S, Liu Y, Cen Z (2008) Lower bound shakedown analysis by using the element free Galerkin method and non-linear programming. Comput Method Appl M 197 (45–48):3911-3921. doi:http://dx.doi.org/10.1016/j.cma.2008.03.009
45. Yu S, Zhang X, Sloan SW (2016) A 3D upper bound limit analysis using radial point interpolation meshless method and second-order cone programming. Int J Numer Meth Eng. doi:10.1002/nme.5273
46. Zhou S, Liu Y, Wang D, Wang K, Yu S (2014) Upper bound shakedown analysis with the nodal natural element method. Comput Mech 54 (5):1111-1128. doi:10.1007/s00466-014-1043-z
47. Zhou S, Liu Y, Chen S (2012) Upper bound limit analysis of plates utilizing the C1 natural element method. Comput Mech 50 (5):543-561. doi:10.1007/s00466-012-0688-8
48. Do HV, Nguyen-Xuan H (2017) Limit and shakedown isogeometric analysis of structures based on Bézier extraction. European Journal of Mechanics - A/Solids 63:149-164. doi:http://doi.org/10.1016/j.euromechsol.2017.01.004
49. Heitzer M, Pop G, Staat M (2000) Basis reduction for the shakedown problem for bounded kinematic hardening material. J Global Optim 17 (1-4):185-200
50. Seshadri R (1995) Inelastic evaluation of mechanical and structural components using the generalized local stress strain method of analysis. Nucl Eng Des 153 (2–3):287-303. doi:http://dx.doi.org/10.1016/0029-5493(95)90020-9
51. Seshadri R, Mangalaramanan SP (1997) Lower bound limit loads using variational concepts: The m(alpha)-method. International Journal of Pressure Vessels and Piping 71 (2):93-106
52. Mackenzie D, Shi J, Boyle JT (1994) Finite-Element Modeling for Limit Analysis by the Elastic Compensation Method. Comput Struct 51 (4):403-410
53. Ponter ARS, Engelhardt M (2000) Shakedown limits for a general yield condition: implementation and application for a Von Mises yield condition. Eur J Mech a-Solid 19 (3):423-445. doi:10.1016/S0997-7538(00)00171-6
54. Boulbibane M, Ponter ARS (2005) Extension of the linear matching method to geotechnical problems. Comput Method Appl M 194 (45-47):4633-4650. doi:10.1016/j.cma.2004.11.009
55. Chen HF, Ponter ARS (2001) A method for the evaluation of a ratchet limit and the amplitude of plastic strain for bodies subjected to cyclic loading. Eur J Mech a-Solid 20 (4):555-571. doi:10.1016/S0997-7538(01)01162-7
56. Chen HF (2010) Lower and Upper Bound Shakedown Analysis of Structures With Temperature-Dependent Yield Stress. J Press Vess-T Asme 132 (1):273-281. doi:Artn

01120210.1115/1.4000369
57. Lytwyn M, Chen HF, Ponter ARS (2015) A generalised method for ratchet analysis of structures undergoing arbitrary thermo-mechanical load histories. Int J Numer Meth Eng 104 (2):104-124. doi:10.1002/nme.4924
58. Barbera D, Chen H, Liu Y, Xuan F (2017) Recent Developments of the Linear Matching Method Framework for Structural Integrity Assessment. Journal of Pressure Vessel Technology 139 (5):051101-051109. doi:10.1115/1.4036919
59. Gokhfeld DA, Charniavsky OF (1980) Limit analysis of structures at thermal cycling, vol 4. Sijthoff & Noordhoff edn. Alphen aan den Rijn, The Netherlands
60. Leonetti L, Casciaro R, Garcea G (2015) Effective treatment of complex statical and dynamical load combinations within shakedown analysis of 3D frames. Comput Struct 158:124-139. doi:https://doi.org/10.1016/j.compstruc.2015.06.002
61. Frederick C, Armstrong P (1966) Convergent internal stresses and steady cyclic states of stress. The Journal of Strain Analysis for Engineering Design 1 (2):154-159
62. Polizzotto C (2003) Variational methods for the steady state response of elastic–plastic solids subjected to cyclic loads. Int J Solids Struct 40 (11):2673-2697. doi:http://dx.doi.org/10.1016/S0020-7683(03)00093-3
63. ABAQUS (Dassault Systems, Version 6.14, 2014).
64. Carvelli V, Cen ZZ, Liu Y, Maier G (1999) Shakedown analysis of defective pressure vessels by a kinematic approach. Arch Appl Mech 69 (9-10):751-764
65. Zhang T, Raad L (2002) An eigen-mode method in kinematic shakedown analysis. Int J Plasticity 18 (1):71-90. doi:http://dx.doi.org/10.1016/S0749-6419(00)00055-3
66. Francois A, Abdelkader H, An LTH, Said M, Tao PD (2007) Application of lower bound direct method to engineering structures. J Global Optim 37 (4):609-630
67. Belytsch.T (1972) Plane Stress Shakedown Analysis by Finite Elements. Int J Mech Sci 14 (9):619-625
68. Zhang G (1992) Einspielen und dessen numerische Behandlung von Flächentragwerken aus ideal plastischem bzw. kinematisch verfestigendem Material. Ph.D. Thesis, University Hanover, Germany
69. Groβ-Weege J (1997) On the numerical assessment of the safety factor of elastic-plastic structures under variable loading. Int J Mech Sci 39 (4):417-433. doi:http://dx.doi.org/10.1016/S0020-7403(96)00039-2
70. Krabbenhoft K, Lyamin AV, Sloan SW (2007) Bounds to shakedown loads for a class of deviatoric plasticity models. Comput Mech 39 (6):879-888. doi:10.1007/s00466-006-0076-3